Evaluation of Coulomb-Counting-Based SOC Estimation and Correction Strategies for LFP-Based Heavy-Duty Vehicle Battery Management Systems

Master's Thesis

Muruiqing Guo

Evaluation of Coulomb-Counting-Based SOC Estimation and Correction Strategies for LFP-Based Heavy-Duty Vehicle Battery Management Systems

THESIS

submitted in partial fulfillment of the
requirements for the degree of

MASTER OF SCIENCE

in

ELECTRICAL ENGINEERING

by

Muruiqing Guo

DC systems, Energy conversion & Storage Research Group
Department of Electrical Engineering
Faculty EEMCS, Delft University of Technology
Delft, the Netherlands
www.ewi.tudelft.nl

Maxwell and Spark
Schuttevaerweg 21
Rotterdam, the Netherlands
maxwellandspark.com

Evaluation of Coulomb-Counting-Based SOC Estimation and Correction Strategies for LFP-Based Heavy-Duty Vehicle Battery Management Systems

Author: Muruiqing Guo
Student id: 6141226

Abstract

Accurate state of charge (SOC) estimation is essential for battery management systems (BMSs) in heavy-duty vehicles (HDVs), where batteries are exposed to high voltage and current stress, heavy loads, and dynamic operating conditions. In the context of company-oriented BMS development, the SOC estimator should be accurate, suitable for real-time embedded implementation, scalable to large battery systems, and transparent enough for engineering validation. Lithium iron phosphate (LFP) batteries are attractive in HDV applications because of their safety, relatively low cost, and long cycle life, but the long plateau region in the voltage–SOC curve limits the reliability of voltage-based SOC correction and calibration. For this reason, Coulomb Counting (CC) is selected as the basic SOC propagation framework in this thesis. CC is practical and industrially relevant because it directly uses measured current and has low computational burden, but its sensitivity to initial SOC, current measurement error, and battery capacity mismatch creates challenges for reliable BMS implementation.

The thesis develops a Simulink-based benchmark framework to evaluate selected CC-based SOC estimation and correction strategies for LFP batteries under heavy-duty vehicle operating conditions. A conventional CC estimator, two literature-based correction methods, an improved bias-compensation strategy, and a bias-capacity-aware correction method developed in this thesis are implemented and compared under controlled error cases. The results show that no single correction mechanism is optimal under all conditions: initial SOC correction depends on voltage observability, cycle-level capacity correction is more effective under capacity mismatch, and current-bias compensation is necessary when current sensor drift causes accumulated SOC error. These findings demonstrate that reliable CC enhancement for LFP-based heavy-duty battery systems requires not a stronger correction mechanism, but one matched to the dominant error source and constrained by the reliability of the available correction signals. The benchmark provides an early-stage evaluation platform for future company BMS development, supporting the selection of correction strategies before experimental validation and embedded implementation.

Thesis Committee:

Chair:	Dr. Gautham Ram Chandra Mouli, Faculty EEMCS, TU Delft
University supervisor:	Dr. Hani Vahedi, Faculty EEMCS, TU Delft
Company supervisor:	Mr. Rasoul Faraji, Maxwell and Spark
Committee Member:	Dr. Paul A. Procel Moya, Faculty EEMCS, TU Delft

Preface

The thesis marks the completion of my master's program at TU Delft. The work was carried out in collaboration with Maxwell and Spark and focuses on SOC estimation and correction strategies for LFP-based heavy-duty vehicle battery management systems.

I would like to express my sincere gratitude to my university supervisor, Dr. Hani Vahedi, for his guidance, feedback, and support throughout the graduation project. His comments and advice helped me clarify the research question, improve the structure of the thesis, and develop a more critical understanding of the topic.

I would also like to thank my company supervisor, Mr. Rasoul Faraji, and the team at Maxwell and Spark for providing me with the opportunity to work on the industry-oriented topic. Their practical insights offered me a better understanding of the difference between academic algorithm development and practical BMS implementation. I am also grateful for the warm and supportive working environment I experienced during my first internship.

I would also like to thank Dr. Gautham Ram Chandra Mouli and Dr. Paul A. Procel Moya for serving as members of the thesis committee and for the time and support during the final assessment process.

I am grateful for the support and encouragement from my friends, which brought me a lot of joy. Finally, I would like to thank my family for their continuous understanding and care throughout my studies.

Muruiqing Guo
Delft, July 17, 2026

Contents

List of Figures

Chapter 1

Introduction

1.1 Electrification of Heavy-Duty Road Transportation

Heavy duty vehicles (HDVs), including trucks, buses, and coaches, are responsible for more than a quarter of greenhouse gas (GHG) emissions from road transport in the European Union (EU) and contribute over 6% to total EU GHG emissions according to the ACEA fact sheet [1]. In response to the disproportionate environmental impact, the EU proposed a regulation regarding CO2 emission that sets the target of reducing average GHG emissions by at least 55% by 2030 compared to 1990 levels [2]. To meet these regulatory emissions targets and environmental calls, the electrification of heavy-duty road transport has become a key issue in both Europe and beyond.

However, electrification is not simply achieved by replacing only the architecture of the propulsion and energy systems. The high energy demand and intensive operating conditions impose demanding requirements on energy storage systems, making the performance and management of battery systems the central problem in electrification.

1.2 Heavy-Duty Battery Systems and BMS Requirements

Compared to light-duty electric vehicles (EVs), such as passenger cars, HDVs require significantly higher energy storage capacity and power delivery due to their larger vehicle mass, payload requirements, longer operating hours, and more intensive duty cycles [3, 4]. Depending on the application, their operation can often involve frequent acceleration and regenerative braking, resulting in a dynamic discharge current profile [5]. These conditions require more robust battery systems with high power capability and reliable operation during extended periods.

To meet these requirements, HDV battery packs often employ either high-voltage or high-current architectures and include a large number of cells connected in series and/or parallel. While this battery configuration offers the necessary power and energy, it also brings more challenges to the monitoring, sensing, balancing, and protection of the battery pack. Therefore, the electrification of HDVs depends not only on robust hardware, but also on a reliable and durable control mechanism to ensure smooth operation. In this context, the battery management system (BMS) becomes critical as it connects battery measurements with control, protection, and communication decisions at the system level.

Although there is no universally accepted definition of a BMS, it is typically considered any system designed to take care of a battery's operation, safety and longevity [6]. In vehicle applications, its main functions can be summarized as monitoring, state estimation, protection, balancing, thermal management, fault diagnosis, and communication [7, 8, 9, 10, 11, 12, 13]. These functions allow the BMS to process measured signals and support safe, efficient, and reliable battery operation under varying load, temperature, and aging conditions.

A typical BMS architecture is illustrated in Figure 1.1. The BMS receives measured signals such as cell voltage, pack voltage, pack current, and temperature. These measurements are used for battery state estimation, protection decisions, balancing control, thermal management, and communication with higher-level vehicle controllers through interfaces such as CAN communication [14].

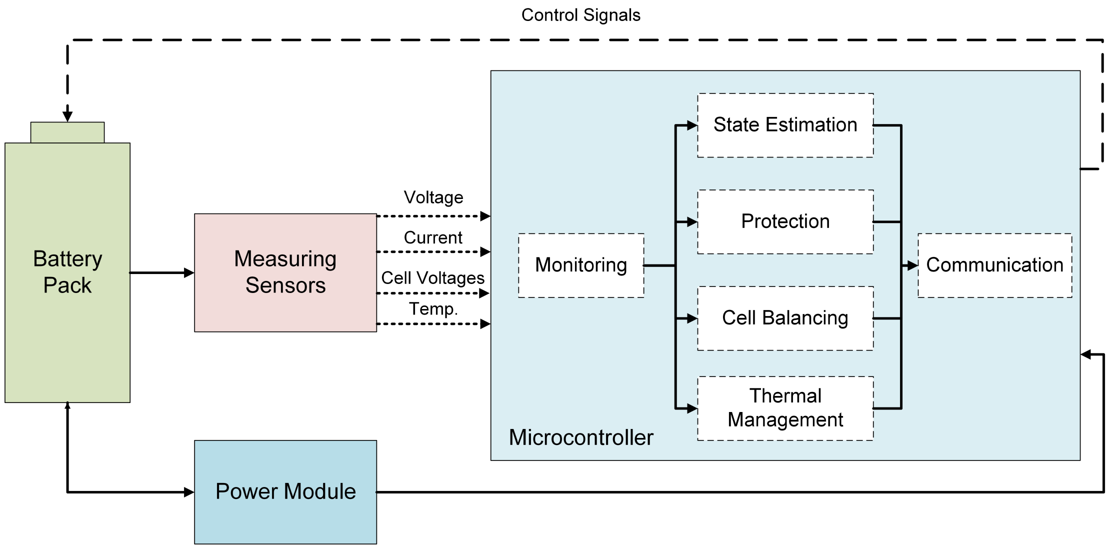

Figure 1.1: General architecture of a battery management system. Adapted from [14].

Among all the functions of BMS, battery state estimation is a vital task because many control and protection decisions depend on the estimation of the battery internal state. In particular, state of charge (SOC) estimation is one of the most important state estimation functions. SOC represents the remaining charge of the battery and is closely related to usable energy, charging decisions, and protection actions [15].

In heavy-duty applications, where vehicle operation is strongly tied to BMS functions, an inaccurate SOC estimation may lead to unsuitable charging decisions, conservative or even extreme available capacity usage. Therefore, reliable SOC estimation under dynamic operating conditions is an important requirement for heavy-duty vehicle electrification. For a company-developed BMS, the SOC estimator should also be suitable for real-time embedded implementation, scalable to large battery packs with many cells and modules, and transparent enough for engineering validation [13, 16].

1.3 Challenge of $LiFePO_4$ Batteries for SOC Estimation

The difficulty of SOC estimation is strongly dependent on the battery chemistry and its electrochemical characteristics. For heavy-duty vehicle applications, the choice of battery chemistry is not determined by energy density alone. Safety and cycle life are more important factors because, compared to EVs, HDVs pose challenges on the safety and durability of battery packs. Lithium-ion batteries consist of several different chemistries such as lithium nickel manganese cobalt oxides (NMC), lithium nickel cobalt aluminum oxides (NCA), and lithium iron phosphate (LFP). Table 1.1 summarizes the representative trends of major lithium-ion battery chemistries based on literature and market reports [17, 18, 19, 20].

Table 1.1: Indicative comparison of representative lithium-ion battery chemistries

Property	**LFP**	**NMC**	**NCA**
Specific energy (Wh/kg)	90–160	150–250	200–260
Volumetric energy density (Wh/L)	300–400	500–700	550–750
Cycle life	3000–5000	1000–2000	1000–2000
Thermal stability	High	Moderate	Low
Safety	Excellent	Good	Fair
Low-temperature performance	Poor	Good	Good
Relative cost	Lower	Higher	Higher

Note: The numerical values are indicative ranges. They vary with manufacturer, cell format, operating condition, temperature, depth of discharge, and production year.

As shown in Table 1.1, compared to NMC and NCA, LFP generally offers longer cycle life, higher thermal stability, stronger safety characteristics, and lower relative cost, although with lower energy density and weaker low-temperature performance [21, 22]. This trade-off is particularly relevant for HDV applications, where batteries are large, expensive, and exposed to intensive operating schedules. Therefore, LFP is considered suitable for the electrification of heavy-duty vehicles.

From an SOC-estimation perspective, however, the key limitation of LFP is its low voltage-SOC sensitivity in the flat plateau region [23, 24, 25]. Figure 1.2 shows the dynamic charging and discharging curves of EVE battery LF100LA based on the product specification data provided by the manufacturer.

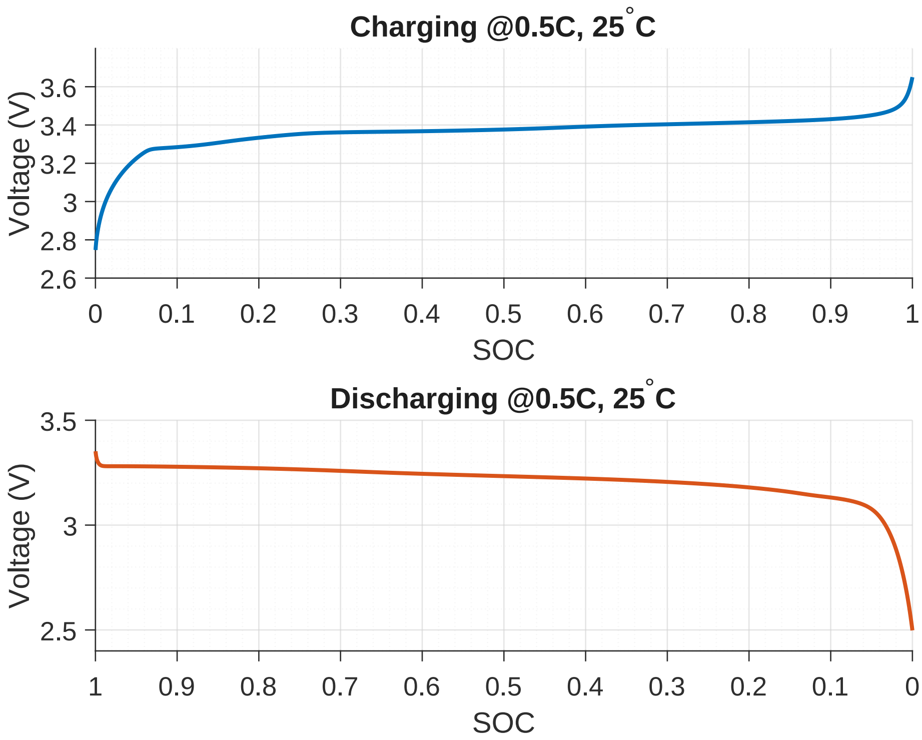

Figure 1.2: Dynamic charging and discharging voltage curves of the LF100LA LFP cell at 0.5C and 25°C.

As shown in Figure 1.2, the cell voltage changes only slightly over a wide SOC region (~20% to 80%). As a consequence, a small voltage variation may correspond to a large SOC interval, bringing more difficulty to SOC estimation and calibration. In addition, during dynamic operation, the measurement of terminal voltage will also be influenced by current, internal resistance, temperature, polarization, and relaxation effects, which means that during operation, voltage measurements alone are insufficient for accurate SOC estimation [22]. This limitation motivates the use of current-based SOC propagation, especially Coulomb Counting, which is discussed from an industrial BMS perspective in the following section.

1.4 Industrial Motivation for CC-Based SOC Estimation

The LFP voltage plateau discussed in the previous section limits the reliability of voltage-based SOC estimation and correction over a wide SOC range. For a company-developed BMS, the SOC estimator must operate in real time, rely on continuously available measurements, scale to large battery packs with many cells and modules, and remain transparent for engineering validation. Since pack current is a standard measured signal in a BMS, current integration provides a practical basis for tracking the charge entering and leaving the battery pack.

This practical choice is consistent with existing industrial battery-management and battery-monitoring products. For example, the Orion BMS describes its SOC calculation as primarily tracking the current entering and leaving the battery, which is Coulomb Counting [26]. Similarly, commercial battery monitors such as the Victron SmartShunt determine the net charge added or removed by measuring and integrating the current flow [27]. At the fuel-gauge IC level, Texas Instruments describes gas-gauge devices that include ADC-based Coulomb counters together with voltage and temperature measurements [28]. These examples show that Coulomb Counting is an industrial building block for practical battery state estimation. As a consequence, this thesis selects CC as the basic SOC propagation framework.

1.5 Problem Statement and Research Gap

After selecting CC as the basic SOC propagation framework, its accumulated error becomes the main technical problem addressed in this thesis. SOC estimation directly affects energy management, charging decisions, protection limits, and the usable capacity reported to the vehicle-level controller. Therefore, the limitations of CC must be understood before CC-based SOC estimation can be applied to LFP-based HDV battery systems.

Since CC relies on open-loop current integration, its accuracy depends on the initial SOC, current measurement accuracy, available capacity, Coulombic efficiency, and sampling or timing accuracy. Errors in these quantities can accumulate over time and lead to SOC drift. Movassagh et al. [29] systematically analyzed the possible error scenarios that might occur in real CC applications. The mismatch of initial SOC, the drift in current measurement sensor, and battery aging can all contribute to an incorrect SOC estimation. In real heavy-duty vehicle operations, these error cases may become more relevant over long operating periods, repeated cycles, and battery aging problems, adding uncertainty to SOC estimation.

Several studies have proposed various enhancement or correction methods for different types of errors. Das et al. [30] proposed a least-squares-regression-based algorithm using standby windows to correct the initial SOC before the calculation begins. Lee and Won [31] introduced a method that estimates battery capacity and Coulombic efficiency of each cycle, combining with an SOC reset from OCV inversion at the beginning of the cycle.

However, there are two gaps. First, existing CC calibrations and corrections are often developed and verified under different assumptions and settings. In other words, there is no systematic comparison for these enhancement methods within a common framework under the same battery model, error cases and evaluation metrics. Second, many existing CC enhancement and SOC correction methods are developed or validated using battery chemistries such as NMC or NCA, often under operating profiles that are not specifically representative of heavy-duty vehicle applications. Their performance cannot be directly assumed for LFP-based HDV battery systems, because of the plateau region of LFP and the dynamic operation profiles of HDVs. Therefore, the applicability and limitations of these methods in the LFP-based HDV context are not sufficiently understood.

1.6 Research Question and Thesis Structure

Based on the research gaps, the main research question of the thesis is:

> How do selected CC-based SOC correction methods compare in terms of estimation accuracy and applicability under representative LFP-based heavy-duty vehicle operating and error scenarios?

This main question leads to three sub-questions:

1. How can an existing Simulink battery example be adapted into a unified benchmark for evaluating CC-based SOC estimation and enhancement methods for LFP batteries under dynamic heavy-duty operating conditions?
2. How do the selected CC-based enhancement methods perform compared with basic Coulomb Counting under the same battery model, operating profile, error scenarios, and evaluation metrics?
3. What are the advantages, limitations, and applicable conditions of these methods for LFP-based heavy-duty battery management systems?

The structure of the thesis is constructed as follows. Chapter 2 explains the technical background of BMS, SOC estimation, Coulomb Counting, and its error mechanisms. Chapter 3 develops the Simulink example into a unified benchmark platform by defining the battery model, operating cycles, error injection cases, and evaluation metrics. Chapter 4 introduces the selected CC-based correction methods from literature and explains how they are implemented or adapted in the benchmark. Chapter 5 evaluates the methods under the predefined benchmark cases and presents the simulation results. Chapter 6 summarizes the main conclusions, answers the research questions, and points out future work.

Chapter 2

Coulomb Counting and Error Mechanisms

This chapter introduces the technical background required for SOC estimation in the thesis. Since Chapter 1 has introduced the practical motivation for selecting CC-based SOC estimation in a company-developed LFP/HDV BMS context, this chapter further explains the technical background of CC. First, representative SOC estimation methods are briefly reviewed to position CC among alternative approaches. Then, the continuous-time and discrete-time formulations of Coulomb Counting are derived. Finally, the main error mechanisms of CC are analyzed, which motivate the benchmark error scenarios used in the following chapters.

2.1 Overview of State of Charge (SOC) Estimation Methods

Battery state estimation refers to the calculation of the battery's current state and the prediction of future performance that cannot be directly measured from the sensors [32]. Typical examples include state of charge (SOC), state of health (SOH) and state of power (SOP). Among them, SOC is the most critical one because it is directly related to the energy usage of the battery and therefore is a vital input for thermal management and protection [15, 33].

SOC is commonly defined as the ratio between the remaining available charge and the maximum available capacity:

$$\mathrm{SOC}(t) = \frac{Q_{\mathrm{avail}}(t)}{Q_{\mathrm{n}}} \tag{2.1}$$

It is an indicator of how much energy is stored in the battery at the moment. SOC estimation is used to determine when to charge or discharge the battery, optimize the charge and discharge strategy, and prolong the battery life.

SOC estimation algorithms can be generally divided into four categories [32]. These categories are briefly reviewed in the following sections.

2.1.1 Open-Circuit Voltage (OCV) Mapping

OCV-based method estimates SOC according to the look-up table of the relationship between the voltage and the SOC. The look-up table can be obtained by measuring the static voltage in different SOC states. During the actual operation, SOC is determined based on its position on the OCV–SOC curve.

OCV-based estimation is the simplest method compared to other methods. However, the OCV–SOC relationship can be influenced by multiple factors such as battery aging and different temperatures, and therefore will easily lose its accuracy after several cycles [34]. Also, for LFP batteries, the flat OCV–SOC plateau reduces the sensitivity of SOC to voltage over a wide operating range. As a result, the OCV mapping is used as a correction method rather than a standalone estimator during dynamic operation [22, 35].

2.1.2 Coulomb Counting

This method estimates battery SOC by counting the amount of charge (coulombs) entering or leaving the battery. The calculation is simple; as long as the starting point is known, the integration during operation could give the estimation result at the endpoint. Section 2.2 will explain the mechanism in detail.

Coulomb Counting stands out because of its simplicity and accuracy especially in the short term. Its inputs only contain initial SOC, current and battery capacity. The main limitation of Coulomb Counting, however, is that the accuracy highly depends on the initial SOC, current measurement, battery capacity, and sampling time [36]. Therefore, the error mechanisms should be considered in advance and different calibration methods are proposed.

2.1.3 Model-Based Observer Method

Model-based observer methods estimate SOC by combining the measured signals with a battery model [37]. Equivalent circuit models (ECMs), such as the Rint model, first-order RC model and second-order RC model, are commonly used to describe the dynamic response of the battery.

The selected battery model is used by an observer or filter to estimate internal states that cannot be directly measured. Common observers include the Kalman Filter (KF), Extended Kalman Filter (EKF), Particle Filter (PF), and sliding mode observer [38]. Typically, these observers compare the voltage measurement and estimation to estimate SOC, and the error is then sent back to the observer for correction.

Model-based observer methods can improve SOC estimation by correcting the accumulated error that may occur in open-loop methods such as Coulomb counting. However, their performance depends strongly on the accuracy of the battery model, the model parameters, and observer tuning. As a result, although model-based observer methods are widely used in advanced BMS applications, they usually require more modeling effort and computational resources than simple Coulomb-Counting-based methods. Recent LFP studies further show that observer-based estimators may require bias compensation or adaptive correction because the flat OCV–SOC curve weakens voltage-based observability and increases sensitivity to measurement bias [35].

2.1.4 Data-Driven Methods

Data-driven methods estimate SOC by learning the relationship between measurable battery signals and SOC from pre-obtained experimental and/or operational data. Eleftheriadis et al. [39] describe different categories of data-driven methods in detail. These methods can be classified into different groups such as Support Vector Machine (SVM), Gaussian Process Regression (GPR) and Neural Network (NN). Recent studies have further explored machine-learning and physics-informed deep-learning models for SOC estimation using measured voltage, current, and temperature sequences, including LFP-specific approaches designed to address the flat OCV–SOC platform [39, 40].

Compared with model-based methods, data-driven algorithms are black-box models that do not require clearly predefined physical models. Instead, battery behavior is learned from data. This allows them to deal with more complicated non-linear cases as long as the captured data are sufficient. In contrast, the strict requirement for a large amount of training data makes validation and calculation more challenging.

The SOC estimation methods reviewed above differ in their required inputs, implementation complexity, dependence on battery-specific data, and correction capability. They are not completely independent in practical BMS applications because CC can be used as the basic SOC propagation method, while OCV correction, model-based observers, or data-driven compensation can be introduced to reduce accumulated errors. The following section introduces the principle of Coulomb Counting and the main error sources that affect its estimation accuracy.

2.2 Coulomb Counting Principle

2.2.1 Continuous Time Calculation

Assume that positive current refers to charging. Coulomb Counting can be derived from the relationship between battery charge and terminal current:

$$I(t) = \frac{\mathrm{d}q(t)}{\mathrm{d}t} \tag{2.2}$$

For a rechargeable cell, we are interested in its reversible, usable charge, which is defined here as $Q_{avail}(t)$. The rated capacity Q_n (Ah) is defined under a specific test condition as the total amount of charge that can be extracted when the cell is discharged from full to the cut-off voltage. By definition:

$$Q_n = -\frac{1}{3600}\int_{t_{full}}^{t_{cutoff}} I(t)\,dt \tag{2.3}$$

When the battery pack is charged, the available capacity increases; when it is discharged, the available charge decreases. In addition, not all terminal charge contributes to the reversible capacity due to side reactions and inefficiencies. This phenomenon is captured by coulombic efficiency $\eta(t) \in (0,1]$. Therefore, the time derivative of the available capacity

$$\frac{\mathrm{d}Q_{\mathrm{avail}}(t)}{\mathrm{d}t} = \frac{\eta(t)\,I(t)}{3600} \tag{2.4}$$

Combining this with the definition of SOC Eq. (2.1) gives

$$Q_\mathrm{n}\frac{\mathrm{dSOC}(t)}{\mathrm{d}t}=\frac{\eta(t)\,I(t)}{3600} \tag{2.5}$$

Hence, the continuous-time SOC dynamics

$$\frac{\mathrm{dSOC}(t)}{\mathrm{d}t}=\frac{\eta(t)}{3600Q_\mathrm{n}}I(t) \tag{2.6}$$

The integral form

$$\mathrm{SOC}(t)=\mathrm{SOC}(t_0)+\frac{1}{3600Q_n}\int_{t_0}^{t}\eta(\tau)I(\tau)\,d\tau \tag{2.7}$$

This is the fundamental continuous-time equation behind Coulomb Counting.

2.2.2 Discrete-Time Implementation for BMS

The battery management system operates in a discrete time with a sampling period Δt. During a sampling interval $[t_{k-1},t_k]$, the current can be approximated as a constant value I_k. Therefore, the charge increment

$$\Delta q_k \approx I_k\,\Delta t \quad [\mathrm{C}] \tag{2.8}$$

In practice, the rated capacity Q_n is specified in ampere-hours (Ah), while the current is measured in ampere (A) and time in seconds (s). To work in Ah, the charge increment is converted as

$$\Delta Q_k=\frac{I_k\Delta t}{3600} \quad [\mathrm{Ah}], \tag{2.9}$$

because $1\,\mathrm{Ah}=3600\,\mathrm{C}$.

Convert the continuous-time relationship Eq. (2.1) into discrete-time, the equation becomes

$$\mathrm{SOC}_k=\mathrm{SOC}_{k-1}+\frac{\eta_k}{Q_\mathrm{n}}\Delta Q_k=\mathrm{SOC}_{k-1}+\frac{\eta_k\,I_k\Delta t}{3600\,Q_\mathrm{n}} \tag{2.10}$$

Starting from the initial SOC, the cumulative SOC calculation is:

$$SOC_k=SOC_0+\sum_{i=1}^{k}\frac{\eta_i I_i\Delta t}{3600Q_n}. \tag{2.11}$$

Under the chosen sign convention, this updated rule has the desired behavior:

- when $I_k>0$ (charging), the term $\frac{\eta_k I_k\Delta t}{3600\,Q_\mathrm{n}}>0$ and SOC increases;
- when $I_k<0$ (discharging), the term is negative and SOC decreases.

Eq. (2.10) is the recursive update used in the discrete-time BMS application, while Eq. (2.11) shows that SOC estimation is accumulated from the initial SOC and all previous current samples. This cumulative form also reveals the main weakness of Coulomb Counting: errors in the initial SOC, current measurement, coulombic efficiency, sampling time and capacity value may increase the estimation error during accumulation. These error mechanisms are discussed in the following section.

2.3 Error Mechanisms of Coulomb Counting

The discrete-time Coulomb Counting formulation shows that the SOC estimation is obtained by accumulating current over time from an initial SOC value. Therefore, the accuracy of Coulomb Counting depends on multiple factors such as current measurement, initial SOC, and battery capacity.

Movassagh et al. [41] explicitly analyze the major error sources in Coulomb Counting, which will be briefly reviewed in the following sections. These error sources can generally be categorized as either time-cumulative errors or SOC-proportional errors.

2.3.1 Initial SOC Error

Coulomb Counting requires an initial SOC value to start the integration. If the initial SOC is not accurate, the error is directly inherited by all subsequent estimation. Assuming that the current measurement, capacity, efficiency and sampling time are accurate, an initial SOC error can be written as:

$$e_0 = \widehat{SOC}_0 - SOC_0 \tag{2.12}$$

where SOC_0 is the true SOC and $\widehat{SOC}_0$ is the initial SOC used by BMS.

The SOC estimation then contains this offset throughout the entire process:

$$\widehat{SOC}_k = SOC_k + e_0 \tag{2.13}$$

Pure CC does not have a feedback system, and therefore cannot eliminate this kind of error. The initial SOC error is a one-time error at $t = 0$, and will remain as a bias during the Coulomb Counting session. When considered independently, it remains as an offset and can be reduced using a reliable voltage anchor.

2.3.2 Current Measurement Bias

Current measurement error is one of the most important error sources of SOC estimation. When current measurement error is included, the measured current would become

$$\widehat{I_k} = I_k + e_{I,k} \tag{2.14}$$

where I_k is the true current, $e_{I,k}$ is the measurement error and $\widehat{I_k}$ is the value that enters the Coulomb Counting integration.

Substituting the expression into Eq. (2.10) gives

$$e_{\mathrm{SOC},I}(k) = \sum_{i=1}^{k} \frac{\eta_i e_{I,i} \Delta t}{3600 Q_n} \tag{2.15}$$

If the current error comes from a constant current bias, the expression becomes:

$$e_{\mathrm{SOC},I}(k) \approx \frac{\eta b_I k \Delta t}{3600 Q_n} \tag{2.16}$$

where b_I is the constant current bias.

This equation shows that if there is a constant current bias in the current sensor, the error will accumulate in the process and continuously increase the estimation error.

2.3.3 Capacity Mismatch

Coulomb Counting also depends on the battery capacity value used in the integration. Batteries gradually age during operation, and therefore the capacity will drop as operating time increases. However, if the estimator still uses the nominal capacity Q_n for estimation, the mismatch between the actual battery capacity and the capacity used in the calculation introduces error to SOC estimation. The SOC calculation can be expressed as:

$$\widehat{SOC}_k = \widehat{SOC}_{k-1} + \frac{\eta_k I_k \Delta t}{3600\widehat{Q}_n} \tag{2.17}$$

If $\widehat{Q}_n > Q_n$, the estimator underestimates the SOC change for a given period of time. Unlike current bias, capacity mismatch is not time-cumulative, because it is also related to the accumulated SOC change. [41] classified it as an SOC-proportional error source.

2.3.4 Secondary Error Sources: Efficiency, Integration Approximation, and Timing

In addition to the mentioned error sources, Coulomb Counting can also be affected by Coulombic efficiency, current integration approximation, and timing uncertainty. The current integration approximation error is due to the transfer from continuous current integral to discrete samples in real operation, for example using a rectangular approximation. This error becomes more relevant when the current significantly changes within one sampling interval. Timing uncertainty, in contrast, refers to error in the sampling duration itself, such as oscillator drift or synchronization error. Although both effects are related to the discrete-time implementation, they have different physical meanings.

The uncertainty of the Coulombic efficiency is another possible source of error. It represents uncertainty in the fraction of terminal charge that contributes to reversible charge storage. If the assumed efficiency differs from the actual efficiency, the SOC change during charging or discharging would be incorrect.

Movassagh et al. [41] identify current integration approximation error, Coulombic-efficiency uncertainty, and timing oscillator error as possible Coulomb Counting error sources. However, these effects are not independently varied in the benchmark of this thesis. The sampling time and numerical integration setting are fixed by the simulation environment, and the Coulombic efficiency is assumed to be close to unity under the considered operating conditions. Therefore, the benchmark focuses on the dominant and controllable error sources: initial SOC error, current measurement bias, and capacity mismatch.

2.3.5 Summary of Error Mechanisms

The error mechanisms discussed above affect Coulomb Counting in different ways. Table 2.1 summarizes the main effects and the specific treatment in the thesis.

Table 2.1: Coulomb Counting error mechanisms and benchmark treatment

Error source	**Main effect**	**Treatment in this thesis**
Initial SOC error	Persistent offset	Injected as initial SOC mismatch
Current measurement bias	Time-cumulative drift	Injected as current sensor bias
Capacity mismatch	Throughput-dependent scaling error	Injected as capacity mismatch
Integration, efficiency, and timing uncertainty	Secondary implementation/scaling errors	Discussed; not independently varied

Chapter 3

BMS Modeling in Simulink: Benchmark Framework and Model Adaptation

This chapter introduces the Simulink-based benchmark framework used for the simulation study in the thesis. The simulation framework used in this thesis is derived from the MathWorks *Battery Management System Demo* for MATLAB/Simulink R2022b [42]. The theoretical background and SOC estimation have been introduced in Chapter 2, and this chapter is intended to describe how these concepts are represented in the selected Simulink model.

3.1 Benchmark Framework and Simulation Environment

The Simulink demo used in the thesis provides a reference environment for model-based BMS development and includes battery pack modeling, thermal effects, current limit calculation, SOC estimation, cell balancing, and fault management. The top-level structure of the benchmark model is shown in Figure 3.1.

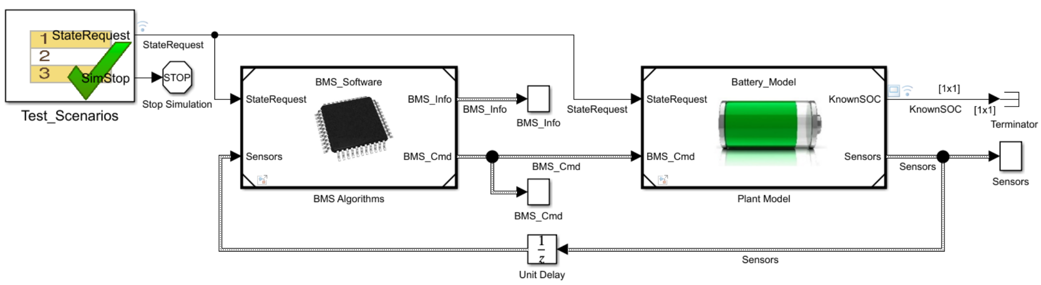

Figure 3.1: Top-level structure of the Simulink-based BMS benchmark framework adapted from the MathWorks Battery Management System Demo [42].

As shown in the figure, the top-level model consists of three main parts: the test scenarios, the BMS algorithms, and the battery plant model. The `Test_Scenarios` block provides the requested system state through the `StateRequest` signal. This signal is passed to both the BMS algorithm subsystem and the plant model, so that the controller and the physical battery model operate under the same requested mode.

The `BMS Algorithms` subsystem represents the software part of the BMS. It receives the `StateRequest` signal and the sensor feedback from the plant model. Based on these inputs, it generates two main output buses: `BMS_Info` and `BMS_Cmd`. The `BMS_Info` bus contains monitoring and diagnostic information, such as estimated SOC, current limits, BMS state, and fault-related signals. The `BMS_Cmd` bus contains control commands sent to the plant model, such as contactor commands and balancing commands.

The `Battery_Model` subsystem represents the physical battery plant. It receives the BMS command bus and the state request, and returns the sensor bus to the controller. The sensor feedback includes the measured quantities required by the BMS algorithms, such as current, voltage, temperature, and cell-related signals. A unit delay is included in the sensor feedback path to avoid an algebraic loop between the plant model and the BMS controller.

The model also provides a `KnownSOC` output from the plant model. This signal is not a directly measurable quantity in a real battery system, but it is useful in simulation because it can be used as a reference value for evaluating SOC estimation performance. Therefore, the benchmark framework allows the estimated SOC from the BMS to be compared with the known plant-model SOC under identical simulation conditions.

Overall, this top-level structure forms a closed-loop BMS simulation environment. The BMS algorithms process sensor information and generate control commands, while the plant model responds to these commands and returns updated measurements. This closed-loop interaction is important for this thesis because the SOC estimation block is evaluated within the same operating context as the other BMS functions, rather than as an isolated mathematical calculation.

3.2 Battery Pack Configuration and Test Scenario

3.2.1 Battery Cell and Pack Configuration

The battery pack model is based on the A123 ANR26650M1 Li-ion cell parameterization available in the Simscape battery library. The cell has a nominal voltage of 3.3 V and a nominal capacity of 2.341 Ah. The battery pack is built using the `builtBattery` function, constructed from parallel assemblies, modules, and module assemblies.

Each parallel assembly includes six cells in parallel, each module includes six parallel assemblies connected in series, resulting in a 6s6p module. Each module assembly consists of four modules, and the battery pack contains four module assemblies. Therefore, the complete battery pack configuration is 96s6p, leading to a pack nominal voltage of $\tilde{3}16.8$ V and a nominal capacity of 14.046 Ah. The details of the battery pack configuration are summarized in Table 3.1.

3.2.2 Benchmark Test Scenario

The benchmark simulation uses a repeated charge-discharge-standby test scenario to evaluate the SOC estimation during dynamic operation. The test setting is generated by `Test_Scenarios`

Table 3.1: Battery pack configuration used in the benchmark model.

Category	Parameter	Value
Cell	Type	A123 ANR26650M1
	Nominal voltage	3.3 V
	Capacity in Simscape model	2.341 Ah
Module	Cells per parallel assembly	6
	Parallel assemblies per module	6
	Module configuration	6s6p
Pack	Modules per module assembly	4
	Module assemblies per pack	4
	Overall configuration	96s6p
	Total number of cells	576
	Nominal voltage	316.8 V
	Nominal capacity	14.046 Ah
	Approximate nominal energy	4.45 kWh

block, providing the operating states for both BMS algorithms and the battery plant model.

In the thesis, a 10-cycle scenario is used. Each cycle has a duration of 5000 s and consists of three phases: a driving / operating state from the beginning, a charging state afterwards, and finally a standby period. The repeated cycles are set to analyze the redundancy and reliability of Coulomb Counting and the algorithms. The benchmark test scenario is concluded in Table 3.2.

Table 3.2: Benchmark test scenario used in the simulation.

Parameter	Value
Number of cycles	10
Cycle duration	5000 s
Driving/load phase	3500 s
Charging phase	1000 s
Balancing/standby phase	500 s
Total simulation time	50000 s
Scenario type	Repeated charge-discharge-standby cycling

3.2.3 Drive-Cycle Current Characteristics

The current profile used in the simulation is shown in Figure 3.2.

In order to simulate real-world HDV operation, the operating current is applied intermittently. Although the peak current reaches 2 C, the average value of operating current is not as high. Also, the pack current is shown with the charge and discharge current limits preset based on battery parameters. These limits define the allowable current range of the battery pack and are

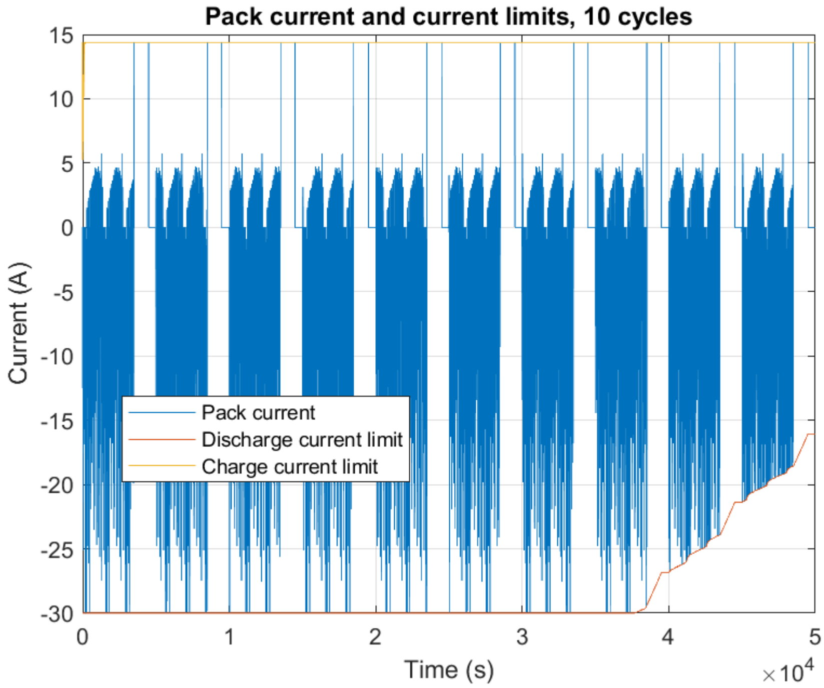

Figure 3.2: Pack current and BMS current limits over the ten-cycle benchmark scenario.

retained as part of the benchmark operating constraints. A representative single-cycle zoom-in is shown in Figure 3.3.

During the driving period, the current profile contains dynamic discharge pulses to simulate the real operating condition, while the charging phase remains the typical CC-CV charging.

To quantify the severity of the current profile, the current signal is evaluated by the pack nominal capacity. The main current characteristics are summarized in Table 3.3.

Table 3.3: Key current characteristics of the benchmark drive cycle.

Quantity	Value
RMS current over ten cycles	9.62 A
RMS C-rate	0.69 C
Initial peak discharge current	-30 A
Initial peak discharge C-rate	2.14 C
Peak charge current	14.4 A
Peak charge C-rate	1.03 C

The current characteristics indicate that the selected profile represents a high-load dynamic operating condition. The initial peak discharge current corresponds to approximately 2.14 C, but the RMS C-rate over the ten-cycle simulation is only about 0.69 C. Therefore, the profile contains short high-power transients without imposing an unrealistically high continuous load

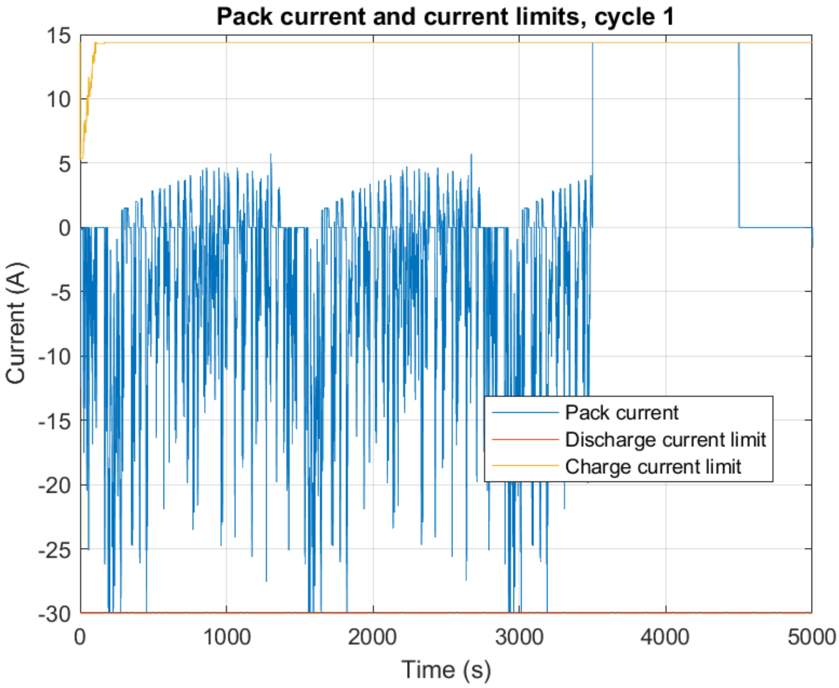

Figure 3.3: Representative single-cycle zoom-in of the pack current and BMS current limits.

on the battery pack. This makes it suitable as an HDV operation current profile for the evaluation of SOC estimation under realistic dynamic conditions.

3.2.4 Voltage and Thermal Operating Context

The cell voltage response is from the battery model settings. The initial SOC is set to 0.98 and slight variations are injected in each parallel assembly to simulate the imbalance that may occur in real operation. The voltage response of the first cycle is shown in Figure 3.4.

As shown in the figure, the initial spread between the cell voltage traces is caused by the intentionally introduced initial SOC differences between the cells. After this, the cell voltages follow the repeated phases of the test scenarios. A relatively flat voltage plateau can be observed during most of each cycle, which is exactly the reason that makes SOC estimation more challenging.

The benchmark model also includes thermal dynamics. During the repeated cycle scenario, the cell temperature gradually increases, leading to a reduction of the allowed discharge current limit in the eighth cycle (as shown in Figure 3.2). This effect is retained as the benchmark setting for the system.

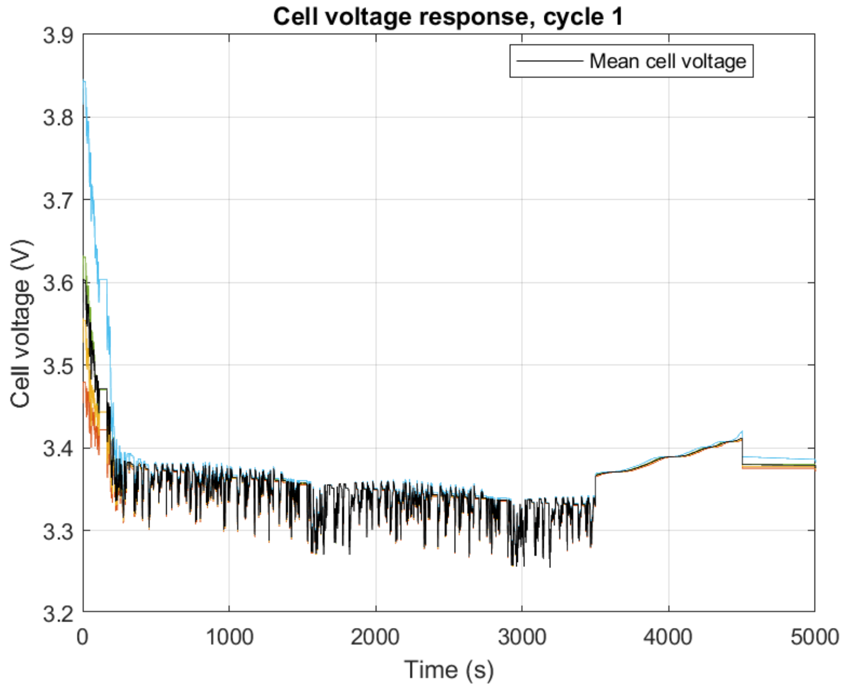

Figure 3.4: Representative single-cycle zoom-in of the cell voltage response.

3.3 SOC Estimation: Coulomb Counting Implementation

After defining the battery pack and test scenario, this section focuses on the Coulomb Counting implementation used in the default BMS model. The theoretical formulation of Coulomb Counting has been introduced in Chapter 2, and this section focuses on how the recursive discrete-time Coulomb Counting equation (Eq. (2.10)) is realized in the model.

3.3.1 Mapping to the Default CC Model

The Coulomb Counting subsystem used in the model is shown in Figure 3.5.

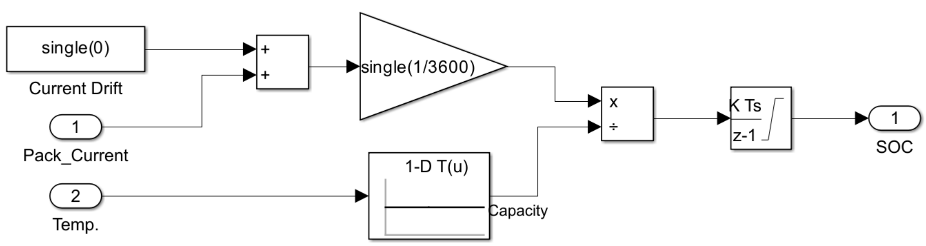

Figure 3.5: Simulink implementation of the Coulomb Counting SOC estimation block in the default BMS model.

As shown in Figure 3.5, the measured pack current is first combined with a current drift input. In the default configuration, this drift input is set to zero, so the estimator uses the measured pack current directly. This input is retained in the subsystem because it allows current bias to be introduced in later simulation cases.

The current signal is then multiplied by the factor $1/3600$, which converts ampere-seconds to ampere-hours. The capacity block provides the nominal battery capacity Q_n used for normalization. The resulting signal represents the SOC rate contribution per unit time, and the discrete-time integrator accumulates this value from the initial SOC SOC_0 using the simulation time step. In this way, the summation implied by the Coulomb Counting equation is realized by the integrator block.

The default BMS model is implemented according to the above recursion. The CC block operates under the following procedure:

1. **Ampere-second to ampere-hour conversion:** Given the measured battery pack current I_k (A) and the simulation time step T_s (s), it computes the capacity change and converts the unit from ampere-second to ampere-hour:

$$\Delta Q_k = \frac{I_k T_s}{3600} \tag{3.1}$$

2. **Capacity normalization and SOC calculation:** Using the nominal capacity of the battery pack Q_n (Ah), the SOC variation

$$\Delta \mathrm{SOC}_k = \frac{\eta_k \Delta Q_k}{Q_\mathrm{n}} = \frac{\eta_k I_k T_s}{3600 Q_\mathrm{n}} \tag{3.2}$$

3. **SOC state update with saturation:** The SOC state is updated as

$$\mathrm{SOC}_k^{\mathrm{raw}} = \mathrm{SOC}_{k-1} + \Delta \mathrm{SOC}_k \tag{3.3}$$

   Moreover, to make sure that the SOC estimation does not exceed the maximum value $\mathrm{SOC}_{\max}$ ($\mathrm{SOC}_{\max} < 1$), a saturation block is added before the final result:

$$\mathrm{SOC}_k = \mathrm{sat}\big(\mathrm{SOC}_k^{\mathrm{raw}}, 0, \mathrm{SOC}_{\max}\big) \tag{3.4}$$

In other words, the default CC model is an exact implementation of discrete-time application. The main difference between the theoretical expression and the Simulink block diagram is that the multiplication by the sampling time is performed inside the discrete-time integrator.

3.3.2 Assumptions Underlying the Default Model

The above derivation relies on the following model assumptions:

1. The rated capacity Q_n is known and constant;
2. The current measurement I_k has no systematic bias;
3. The initial SOC SOC_0 is accurate.

3.4 Model Adaptation for This Study

The original BMS demo contains a large range of editable settings, including contactor management, state-machine control, cell balancing, and fault management. However, the main focus of the thesis is on Coulomb Counting for SOC estimation, so the main adaptation is on the battery model, operating scenario, SOC estimation and data logging setup. Other parts of the BMS are not modified unless relevant to these functions. For example, the charge current limit, discharge current limit and their temperature-dependent behavior were calibrated to reflect the allowable operating range of the battery cells, while the basic logic is kept.

The SOC estimation path is the main part adapted for further analysis. The default CC subsystem is used as a baseline estimator, and additional CC methods are evaluated externally using the same logging signals. The measured pack current, cell voltage, cell temperature, default SOC estimate, and plant-model known SOC are exported from the benchmark model. The known SOC is used only as a simulation reference for evaluating the estimation error and is not treated as a measurable signal in a real BMS.

3.5 Simulation Conditions and Evaluation Signals

The simulation conditions used in the thesis are concluded in Table 3.4.

Table 3.4: Simulation scenario and initial conditions.

Category	Parameter	Value
Scenario	Profile	Ten-cycle repeated charge–discharge
	Cycle duration	5000 s
	Total simulation time	50000 s
Cycle phases	Driving/load phase	3500 s
	Charging phase	1000 s
	Balancing/standby phase	500 s
Initial conditions	Initial SOC	0.98
	Initial temperature	25 °C
BMS constraints	Current limit logic	Voltage- and temperature-dependent

The same simulation conditions are used for all the CC methods considered in the following chapter. This ensures that the performance differences mainly come from the specific mechanisms rather than from the simulation effect.

The main logged signals used for evaluation are the pack current, cell voltages and temperatures, known SOC from the plant model, and the SOC estimation. The pack current is the direct input for CC-based methods. The known SOC is only available in simulation and used for error evaluation.

3.6 Summary

This chapter describes the simulation framework that is based on and adapted from the Simulink demo. The MathWorks demo is adapted to an A123-based LFP battery pack and operates under a repeated charge-discharge-standby scenario for ten cycles. The current profile was considered as a dynamic HDV-based benchmark condition with reasonable values and fluctuations.

The default Coulomb Counting model was implemented based on the recursive discrete-time formula. Additionally, the model adaptation and simulation conditions are introduced, including the retained BMS logic, adjusted operating limits, and logged signals used for evaluation. These settings provide the basic common framework for the method comparison and improvement presented in the next chapters.

Chapter 4

Implemented and Developed CC-Based SOC Estimation and Correction Strategies

This chapter introduces the selected SOC estimation and correction strategies implemented and evaluated in the benchmark. The methods include the conventional Coulomb Counting calculation, two literature-based correction methods, one improvement on the LW method, and the proposed Bias-Capacity-Aware (BCA) strategy. All methods are implemented in the same benchmark so that their correction effects can be evaluated under the same battery model, operating profile, error scenarios, and performance metrics.

The methods are introduced in an order that reflects their correction role: from uncorrected Coulomb Counting to initialization correction, cycle-level correction, current-bias compensation, and finally, bias-capacity-aware correction with region-aware voltage anchoring.

4.1 Method Selection Logic and Correction Targets

The methods in this thesis are selected according to their relationship with Coulomb Counting and their correction targets. A method is considered Coulomb Counting-based if CC remains the primary SOC estimation mechanism, while additional information is used for correction and calibration. Such information may include voltage, resistance, capacity, operating state, operating time, cycle-level capacity throughput, etc. Under this definition, the selected methods are CC-based correction strategies rather than full SOC estimators.

The methods are organized according to their correction roles. Conventional Coulomb Counting provides the uncorrected reference. The DS-inspired method corrects the initial SOC before propagation. The LW method introduces cycle-level correction through parameter update and voltage-anchor reset. The LW-improved method adds a guarded current bias compensation to the original structure. Finally, BCA separates current-bias correction, effective-capacity adaptation, and region-aware voltage anchoring for LFP cells. Table 4.1 summarizes the role of each method in the benchmark.

These methods will be explained in more detail in the following sections.

Table 4.1: Correction role of the implemented SOC estimation strategies

Method	Correction stage	Main role in the benchmark
Conventional CC	No correction	Reference estimator that propagates SOC only by current integration.
DS-inspired method	Before CC propagation	Representative method for initial SOC correction before CC propagation.
LW method	Cycle boundary	Cycle-level correction method for assessing the effect of parameter update and voltage-anchor reset.
LW-improved method	Cycle boundary with bias diagnosis	Extension to test whether adding guarded current-bias estimation improves the LW structure.
BCA method	Propagation and guarded slow update	Developed method for guarded multi-source correction in LFP-based SOC estimation.

4.2 Conventional Coulomb Counting

The conventional Coulomb Counting method is implemented as the baseline estimator in this thesis. It provides the reference SOC trajectory against which all correction strategies are evaluated. The baseline estimator follows the discrete-time current integration principle introduced in Section 2.2. Its main inputs are the battery current, nominal capacity, initial SOC and sampling time.

In the baseline implementation, SOC is propagated only by integrating the measured current over time. No additional voltage-based recalibration, current-bias compensation, capacity adaptation, or cycle-level correction is applied. Therefore, the baseline method represents the simplest CC-based SOC estimation structure and provides a clear reference for evaluating the effect of each added correction mechanism.

The conventional CC baseline is expected to perform well when the initial SOC is accurate, the current measurement has no systematic bias, and the capacity used by the estimator matches the actual usable capacity of the battery. Under these ideal conditions, the error between the estimated SOC and the reference SOC should remain small. However, as discussed in Section 2.3, the baseline method is vulnerable to several practical error sources. An initial SOC error remains as a persistent offset, current measurement bias accumulates over time, and capacity mismatch causes incorrect scaling between charge throughput and SOC variation.

For this reason, conventional CC is not used as an improved method, but as a reference case. The performance difference between conventional CC and correction strategies indicates whether a method can reduce a specific CC error mechanism under the same benchmark conditions.

4.3 DS-Inspired Initial SOC Correction Method

The first literature-based method implemented in this thesis is adapted from the modified Coulomb Counting method proposed by Das et al. [30]. In this thesis, it is referred to as the DS-inspired method. Its role in the benchmark is to represent an initialization-level correction strategy. Instead of changing the CC propagation equation during operation, the method aims to improve the initial SOC before Coulomb Counting begins.

The original study addresses one of the main limitations of conventional CC: the SOC trajectory depends strongly on the initial SOC. Das et al. estimate battery ECM parameters and OCV from terminal voltage and current data using least-squares estimation (LSE). The estimated OCV is then converted into an initial SOC through the OCV–SOC relationship, after which SOC is propagated by Coulomb Counting.

The original study uses experimental pulse-test data from an LFP battery and evaluates both first-order and second-order RC equivalent circuit models. The second-order RC model is finally used for SOC estimation because it represents the terminal voltage dynamics more accurately. In the original procedure, voltage and current data are used to estimate the ECM parameters and the OCV-related term. The estimated OCV is then related to SOC by a fitted OCV–SOC curve. In this way, the method avoids relying only on a direct long-rest OCV measurement, while still using OCV information to determine the initial SOC required by CC.

In this thesis, the DS correction principle is adapted to the unified benchmark simulation. Since the benchmark uses a different battery model, drive-charge-rest operating cycle, signal set, and OCV–SOC table, the implementation is formulated with the available simulated pack and cell signals. A first-order RC approximation is used for the LSE calculation. Local voltage-current windows are used to estimate the OCV-related term and the corresponding R_0-related behavior. The estimated OCV is then mapped to SOC using the benchmark OCV–SOC lookup table, and this corrected SOC is used as the initial value for standard CC propagation. Therefore, in this benchmark implementation, the DS-inspired method modifies the initialization of CC but does not introduce additional current-bias estimation or adaptive capacity correction.

Because the benchmark cell chemistry is LFP, direct OCV–SOC inversion can be unreliable in the flat voltage plateau. To keep the correction physically reasonable, the OCV–SOC inversion is constrained to a local SOC window around the initial CC estimate. This follows the same correction logic as the original method, but adapts the OCV-to-SOC conversion to the observability limitation of the benchmark cell. The resulting benchmark implementation is summarized in Figure 4.1.

The main implementation steps are:

1. collect voltage and current samples from the benchmark simulation;
2. estimate the OCV-related quantity using a first-order RC LSE structure;
3. convert the estimated OCV to initial SOC through the benchmark OCV–SOC lookup table;
4. use the corrected initial SOC as the starting value for standard Coulomb Counting.

In the benchmark, the DS-inspired method represents an initialization-level correction strategy. It is intended to reduce errors caused by an incorrect initial SOC, but it does not explicitly compensate current sensor error or adapt the effective capacity during later operation. Its correction capability also depends on the reliability of OCV–SOC inversion, which can be limited in the flat OCV–SOC plateau region of LFP cells.

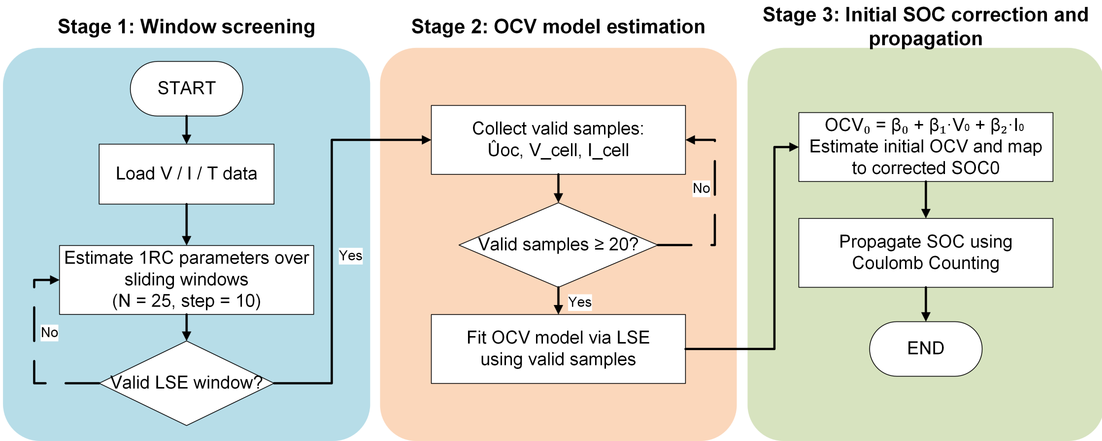

Figure 4.1: Flowchart of the LSE-based OCV initialization correction method.

4.4 LW Cycle-Based Correction Method

The second literature-based correction method is adapted from the cycle-based SOC estimation method proposed by Lee and Won [31]. In this thesis, it is referred to as the LW method. Different from the DS-inspired method, which corrects only the initial SOC, the LW method applies correction at cycle boundaries. It updates correction parameters after each completed cycle and uses them in the next cycle.

This cycle-based correction consists of two main steps. First, the Coulombic efficiency, effective capacity, and internal resistance are calculated from the previous cycle and used for SOC estimation in the next cycle. Second, at the end of each cycle, a voltage anchor is selected and converted into an SOC value through OCV–SOC inversion. This SOC value is used as the initial SOC for the following cycle. The general procedure is summarized in Figure 4.2.

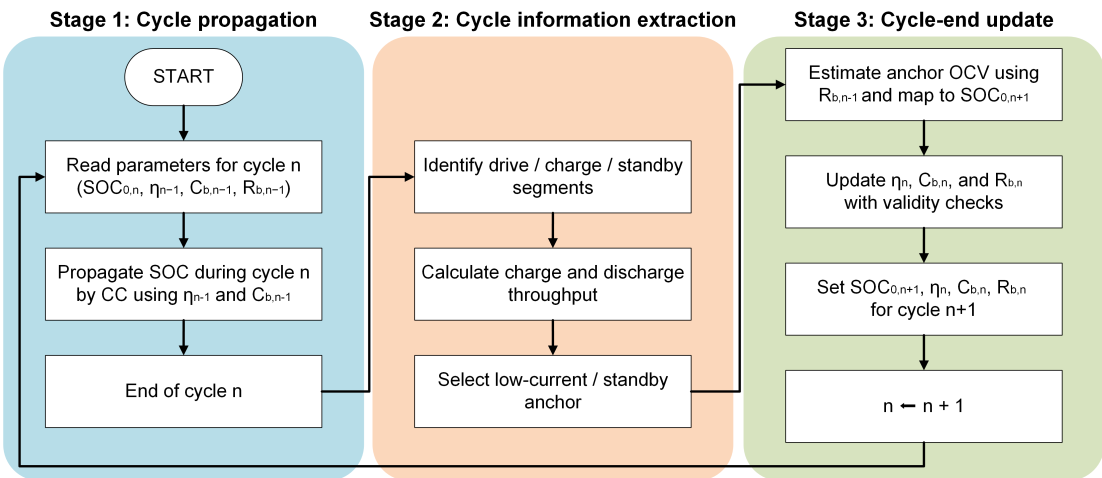

Figure 4.2: Flowchart of the cycle-based correction method.

In the benchmark implementation, the LW capacity update is calculated from the net charge throughput and the SOC change between two cycle anchors. Since the sign convention in this thesis defines positive current as charging, the net discharge throughput in cycle n is calculated as

$$Q_{\mathrm{net},n} = -\frac{1}{3600} \sum_{k \in n} I_{\mathrm{meas},k} \Delta t_k \tag{4.1}$$

The corresponding cycle-level SOC change is calculated from the SOC at the beginning of the cycle and the anchor-derived SOC at the end of the cycle:

$$\Delta SOC_n = SOC_{0,n} - SOC_{\mathrm{anchor},n} \tag{4.2}$$

When $Q_{\mathrm{net},n}$ and ΔSOC_n are sufficiently large and have the same sign, a temporary effective-capacity candidate is calculated as

$$C_{\mathrm{tmp},n} = \frac{|Q_{\mathrm{net},n}|}{|\Delta SOC_n|}. \tag{4.3}$$

The candidate is accepted only when it is finite, positive, within the predefined capacity bounds, and does not exceed the allowed jump from the previous accepted capacity. In addition, consecutive capacity candidates must be sufficiently consistent before the update is activated. When the gate is passed, the effective capacity is updated using

$$C_{b,n} = (1 - \alpha_C) C_{b,n-1} + \alpha_C C_{\mathrm{target},n} \tag{4.4}$$

where $C_{b,n}$ is the effective capacity used for the next cycle, $C_{\mathrm{target},n}$ is the stable capacity target obtained from accepted recent candidates, and α_C is the capacity-update gain.

In the original study, the method was evaluated under controlled experimental conditions, including a standard CC-CV charging process. Under such conditions, the charging and discharging intervals are clearly identified, and the efficiency and capacity calculations can be performed under relatively stable conditions. However, in this benchmark, the current profile is more dynamic to simulate the real operation conditions in HDV application. Therefore, the original update conditions are adapted to the available benchmark signals and cycle definition.

In the thesis, each cycle is defined as three stages: driving, charging, and standby. The net charge throughput is calculated from the measured current over the cycle. A standby anchor is selected at the end of each cycle for the SOC reset. Also, to avoid unrealistic capacity updates, the temporary capacity candidate is accepted only when the net charge throughput, SOC change within each cycle, and jump limit are satisfied. This adaptation keeps the original cycle-based correction approach, while applying the algorithm to the benchmark setting.

In the benchmark, the LW method represents a cycle-level correction strategy. It is intended to reduce accumulated CC propagation error by updating cycle-level parameters and applying a voltage-anchor reset at cycle boundaries. However, since the cycle-level throughput is still obtained from current integration, the method may remain sensitive to persistent current-measurement bias. Its voltage-anchor reset can also be limited when the selected anchor lies in the flat OCV–SOC plateau region of LFP cells.

4.5 LW-Improved Method with Guarded Current-Bias Compensation

The improved LW strategy is developed from a limitation observed in the original LW method. Although the LW method introduces cycle-based capacity and efficiency updates, the charge throughput used in the updates are still obtained by current accumulation. As a result, if a persistent current-measurement bias is present, both the SOC propagation and the parameter update will be affected.

To address this issue, the LW-improved method retains the original mechanisms of cycle-level parameter update and voltage-anchor correction, but adds a guarded current bias estimation mechanism. The added estimator evaluates whether the cycle-level charge inconsistency is consistent with a persistent current-measurement offset. When the inferred bias satisfies the predefined validity conditions, the estimated bias is used to correct the measured current in the following cycle.

The main difference from the original LW method is that LW-improved introduces an explicit current-bias state. In the original LW method, current-measurement bias can only influence the cycle-level throughput and may be indirectly absorbed by parameter updates or anchor resets. In LW-improved, the bias is estimated explicitly from the mismatch between current-integrated charge and anchor-implied charge, and the measured current is corrected before the next cycle propagation.

The current bias is inferred by comparing two cycle-level charge quantities. The first quantity is the charge calculated by integrating the measured current over time, and the second quantity is the charge implied by the SOC change between the initial SOC and the anchor-derived SOC at the end of the cycle. A persistent difference between these two quantities is interpreted as evidence of current-measurement bias. In the implementation, the anchor-implied charge is obtained from the anchor-derived SOC change multiplied by the updated effective capacity. Therefore, the raw bias is calculated as

$$b_{\mathrm{raw},n} = \frac{3600\,(Q_{\mathrm{meas},n} - Q_{\mathrm{anchor},n})}{T_n} \tag{4.5}$$

where $Q_{\mathrm{meas},n}$ is the current-integrated charge in cycle n, $Q_{\mathrm{anchor},n}$ is the anchor-implied charge, and T_n is the cycle duration.

The raw bias is not used directly, because a single-cycle mismatch may also be caused by an unreliable voltage anchor, capacity error, or transient operating condition. Instead, the raw estimate is accepted only when the raw bias exceeds a predefined threshold and has a consistent sign and comparable magnitude across cycles. When these validity checks are satisfied, the filtered bias estimate is updated and used in the following cycle. The corrected current is then given by

$$I_{\mathrm{corr}} = I_{\mathrm{meas}} - \hat{b}_I \tag{4.6}$$

where I_{meas} is the measured current and $\hat{b}_I$ is the filtered current-bias estimate.

Since the original LW cycle-based update procedure is retained, Figure 4.3 only shows the additional bias-compensation logic introduced in the improved strategy.

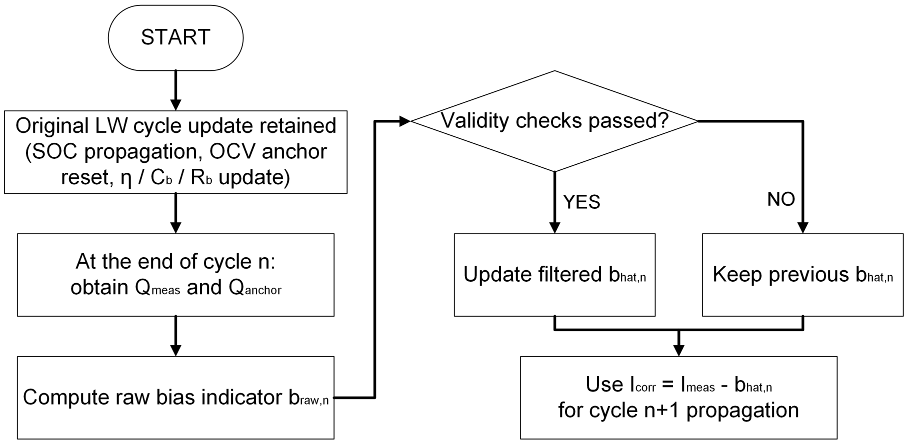

Figure 4.3: Additional guarded bias-compensation logic in the improved LW strategy.

In the benchmark, the LW-improved method represents a bias-compensated extension of the original LW cycle-level correction structure. It is intended to reduce the effect of persistent current-measurement bias while retaining the original LW parameter-update and voltage-anchor mechanisms. Since the bias estimate is accepted only under predefined validity conditions, the method is conservative. It avoids continuous bias correction based on unreliable single-cycle evidence, but it may provide limited correction when the inferred bias is not persistent or when the voltage anchor itself is unreliable.

4.6 Bias-Capacity-Aware (BCA) Correction Strategy

The above two methods both rely on voltage information through OCV–SOC inversion or voltage-anchor reset. However, considering the voltage platform of LFP, this kind of relationship may not be sufficiently reliable. Therefore, a correction strategy that relies too strongly on voltage-derived SOC anchoring may become unreliable for LFP-based SOC estimation.

This motivates the proposed Bias-Capacity-Aware (BCA) strategy. The main design intention is to reduce the dependence on voltage-derived SOC correction and keep the estimator primarily current-driven. Instead of treating voltage as the main correction reference, BCA first corrects the current input and adapts the effective capacity used in Coulomb Counting. Voltage information is used only as a guarded and bounded correction source when the local OCV–SOC relationship is sufficiently informative, i.e. when the operating point is outside the plateau region.

The general structure of the proposed BCA strategy is summarized in Figure 4.4. The method is organized around a current-driven SOC propagation core. The first part is the fast propagation loop, where SOC is updated by Coulomb Counting using a bias-corrected current and the latest effective-capacity estimate. The second part is the slow-state update, where the current bias and effective capacity are updated only when their validity conditions are satisfied. The third part is the optional region-aware voltage-anchor logic, where voltage-derived SOC correction is enabled only when the local OCV–SOC slope is sufficiently informative.

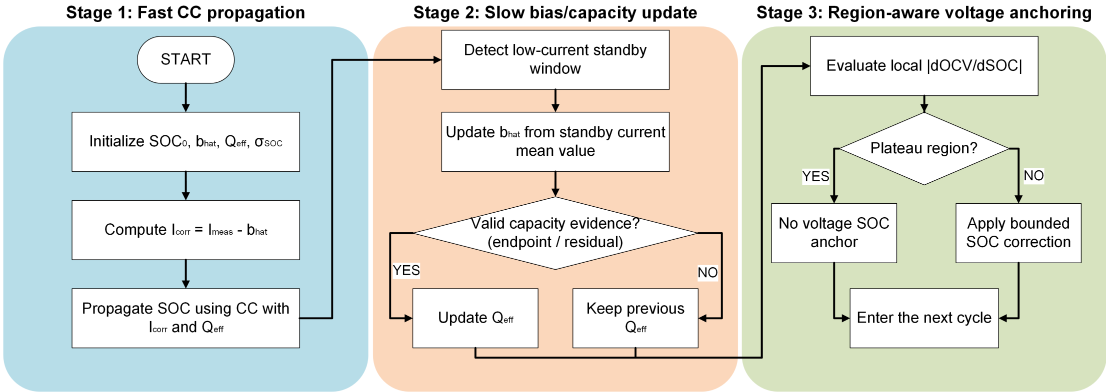

Figure 4.4: Flowchart of the BCA correction strategy.

BCA first focuses on the quantities that directly affect SOC estimation: measured current and battery capacity. Therefore, in the fast propagation loop, SOC is updated using the bias-corrected current and the latest effective capacity estimation. The current bias is estimated from low-current standby windows, where the true current is expected to be close to zero. The effective capacity is represented by a slowly varying capacity scale and can be updated when voltage endpoint information or voltage residuals satisfy the corresponding validity conditions.

Although BCA is designed to reduce dependence on voltage-derived SOC correction, voltage information is not completely discarded. It is used as an optional anchoring source under observability constraints. The direct voltage-derived SOC anchoring is activated only when the local OCV–SOC slope is sufficiently high.

Compared with the LW-based methods, BCA separates the current-bias correction more directly from the voltage-anchor mechanism by estimating bias from standby current instead of from cycle-level anchor mismatch. At the same time, the region-aware voltage gate reduces the risk of applying unreliable OCV–SOC inversion in the LFP plateau.

4.7 Summary of Correction Methods

This chapter introduced the CC-based SOC correction methods implemented in the benchmark. The methods are organized as a progressive set of correction mechanisms. Conventional CC is used as the uncorrected baseline. The DS-inspired method adds initialization-level correction before CC propagation. The LW method introduces cycle-level correction through parameter update and voltage-anchor reset. The LW-improved method retains the original LW mechanism but adds a guarded cycle-level bias-compensation mechanism to reduce sensitivity to persistent current bias. Finally, the developed BCA strategy reduces the dependence on voltage-derived SOC correction by prioritizing current-bias correction and effective-capacity adaptation.

The methods differ mainly in the timing, information source, and target of their correction. The DS-inspired method acts before propagation and targets the initial SOC. The LW-based methods use cycle-level throughput and voltage anchors at cycle boundaries. The BCA strategy keeps the estimator primarily current-driven and treats voltage anchoring as an optional and bounded correction source for LFP cells.

These differences provide the basis for the benchmark comparison in the next chapter. The following results chapter evaluates the methods according to the dominant error source, including initial SOC error, current-sensor bias, effective capacity mismatch, and mixed error conditions. This case-based evaluation shows which correction mechanisms are effective under each error scenario.

Chapter 5

Results and Discussion

This chapter evaluates the conventional Coulomb Counting estimator and the selected CC-based estimation strategies introduced in Chapter 4. The chapter uses a two-level analysis structure. First, the methods are compared under each benchmark error case using common SOC error metrics and trajectory plots. This provides a case-based evaluation of the external estimation performance. Second, selected method-specific diagnostic variables are examined to explain the internal correction mechanisms behind the observed trends because the methods rely on different internal correction variables.

Therefore, the results are organized by error cases, including the baseline condition, initial SOC error, current measurement bias, and capacity mismatch. Each case is analyzed by common SOC metrics, and method-specific indicators are introduced after the case-based comparison when they are helpful to explain why a method improves or fails under a particular error scenario.

5.1 Overview of Evaluated Cases and Metrics

This section summarizes the benchmark error cases and performance metrics used for the comparison. All methods are evaluated under the same battery model, operating profile, and error injection settings. Table 5.1 summarizes the evaluated benchmark cases.

As shown in the table, the benchmark includes one reference case, three single-error groups, and one mixed-error group. The single-error cases are set to isolate the effect of each dominant error source, and the mixed-error cases are used to examine whether different error mechanisms reinforce or compensate each other.

For a fair comparison, all methods use the same SOC error definition and quantitative metrics. The SOC estimation error is defined as

$$e_{\mathrm{SOC},k} = SOC_{\mathrm{est},k} - SOC_{\mathrm{ref},k} \tag{5.1}$$

where $SOC_{\mathrm{est},k}$ is the estimated SOC at time step k and $SOC_{\mathrm{ref},k}$ is the reference SOC obtained from the battery model.

Three quantitative metrics are used in this chapter: root mean square error (RMSE), bias, and maximum absolute error (MaxAbs). The RMSE is used to quantify the overall estimation

Table 5.1: Summary of evaluated benchmark cases

Group	**Case ID**	**Variation**	**Purpose**
Reference	A0	No injected error	Check baseline behavior and whether correction methods introduce unnecessary disturbance.
Initial SOC error	B1–B3	Estimator $SOC_0 = 0.90$; estimator $SOC_0 = 0.85$; reference SOC = 0.80 with estimator $SOC_0 = 0.90$	Evaluate the influence of incorrect SOC initialization and the ability of correction methods to reduce initial offset.
Current bias	C1–C3	$+1$ A; $+0.5$ A; -0.5 A	Evaluate SOC drift caused by systematic current measurement bias, including bias magnitude and direction.
Capacity mismatch	D1–D2	Capacity factor = 0.75; 0.85	Evaluate SOC scaling error caused by mismatch between actual usable capacity and estimator capacity.
Mixed errors	E1–E3	$0.85Q_n + 1$ A; $0.85Q_n + SOC_0 = 0.90$; $SOC_0 = 0.90 +$ 0.5 A	Evaluate method robustness when two practical Coulomb Counting error mechanisms coexist.

error:

$$RMSE = \sqrt{\frac{1}{N}\sum_{k=1}^{N} e_{\mathrm{SOC},k}^2} \tag{5.2}$$

The bias is defined as the mean SOC error over the simulation period:

$$Bias = \frac{1}{N}\sum_{k=1}^{N} e_{\mathrm{SOC},k} \tag{5.3}$$

The MaxAbs is used to capture the worst-case deviation:

$$MaxAbs = \max_{1\le k\le N} |e_{\mathrm{SOC},k}| \tag{5.4}$$

The three metrics describe different aspects of performance. RMSE reflects the overall error level, bias indicates the direction and magnitude of systematic deviation, and MaxAbs captures the largest instantaneous error. Therefore, the comparison in the following sections is based on these three metrics.

In addition to the common metrics mentioned above, method-specific diagnostic indicators will be introduced when needed to explain the internal correction behavior of a method.

5.2 Case A: Baseline Condition

5.2.1 Purpose and Setup

The baseline condition is used as the reference case for evaluating all the implemented methods. In this case, no error is injected, and the initial SOC, measured current, and estimator capacity are consistent with the reference battery model. Therefore, conventional CC is expected to provide the lowest error.

The purpose is to provide a reference condition to verify the basic benchmark behavior and to check whether the calibration mechanisms would introduce unnecessary disturbances when no correction is required.

5.2.2 Results

Table 5.2 shows the quantitative results under the baseline condition.

Table 5.2: SOC estimation error metrics under the baseline condition

Method	RMSE (%)	Bias (%)	MaxAbs (%)
Conventional CC	0.08	0.07	0.14
DS-inspired	1.21	1.21	1.28
LW	0.69	0.64	1.06
LW-improved	0.69	0.64	1.06
BCA	0.56	0.53	0.68

As expected, conventional CC estimation gives the lowest error under the baseline condition, with an RMSE of 0.08% and a MaxAbs error of 0.14%. This is because no additional error is injected, and the assumptions of conventional CC are nearly satisfied. The errors of all other methods are slightly higher than the conventional CC calculation, but all errors remain below 1.5%. This indicates that the additional correction mechanisms do not introduce large artificial disturbances under the no-error condition. Therefore, Case A is used as the reference condition for the following error-injection cases.

5.3 Case B: Initial SOC Error

5.3.1 Purpose and Setup

Case B evaluates the effect of incorrect SOC initialization. Since conventional Coulomb Counting propagates SOC by current integration, an initial SOC error appears as a persistent offset unless an additional correction mechanism is applied. Therefore, this case examines whether the selected methods can reduce an initial offset before or during SOC calculation.

Three initial condition variations are evaluated. In the first two cases, the reference initial SOC is 0.98, while the estimator initial SOC is set to 0.90 and 0.85, respectively. These two cases represent underestimated initial SOC values with different offset magnitudes. In the third case, the reference initial SOC is 0.80, and the estimator initial value is 0.90. This case represents an overestimated initial SOC and also places the battery in the flat OCV–SOC region.

5.3.2 Results

The quantitative results under initial SOC error are summarized in Table 5.3.

Table 5.3: SOC estimation error metrics under initial SOC error

Initial condition	**Method**	**RMSE (%)**	**Bias (%)**	**MaxAbs (%)**
Ref. $SOC_0 = 0.98$, est. $SOC_0 = 0.90$	Conventional CC	7.93	-7.93	8.00
	DS-inspired	1.21	1.21	1.28
	LW	2.62	-0.15	8.00
	LW-improved	2.62	-0.15	8.00
	BCA	2.77	-0.84	8.00
Ref. $SOC_0 = 0.98$, est. $SOC_0 = 0.85$	Conventional CC	12.94	-12.94	13.00
	DS-inspired	1.21	1.21	1.28
	LW	4.17	-0.65	13.00
	LW-improved	4.17	-0.65	13.00
	BCA	6.34	-3.71	13.00
Ref. $SOC_0 = 0.80$, est. $SOC_0 = 0.90$	Conventional CC	10.07	10.07	10.14
	DS-inspired	9.94	-9.94	10.00
	LW	3.16	1.00	10.01
	LW-improved	3.16	1.00	10.01
	BCA	4.25	1.74	10.01

For conventional CC, the initial SOC error appears as a nearly constant offset. When the estimator starts from $SOC_0 = 0.90$ while the reference initial SOC is 0.98, the RMSE is 7.93%. When the estimator starts from $SOC_0 = 0.85$, the RMSE increases to 12.94%. These data confirm that without correction, the magnitude of the initial SOC error directly determines the estimation error level.

The DS-inspired method shows the strongest improvement in the first two cases. Its RMSE remains 1.21% for both underestimated initial SOC cases because the method recalculates the initial SOC from the LSE-based OCV estimate before operation. As a result, the given estimator initial value has limited influence as long as the same valid initialization windows and operating conditions are used.

The third case exposes a different trend. When the reference initial SOC is 0.80 and the estimator initial SOC is 0.90, the DS-inspired method no longer provides clear improvement over conventional CC. This suggests that the effectiveness of OCV-based initial SOC correction depends on the local OCV–SOC observability.

The case with reference $SOC_0 = 0.98$ and estimator $SOC_0 = 0.90$ is selected as a representative example. The SOC trajectories and error comparisons are shown in Figure 5.1.

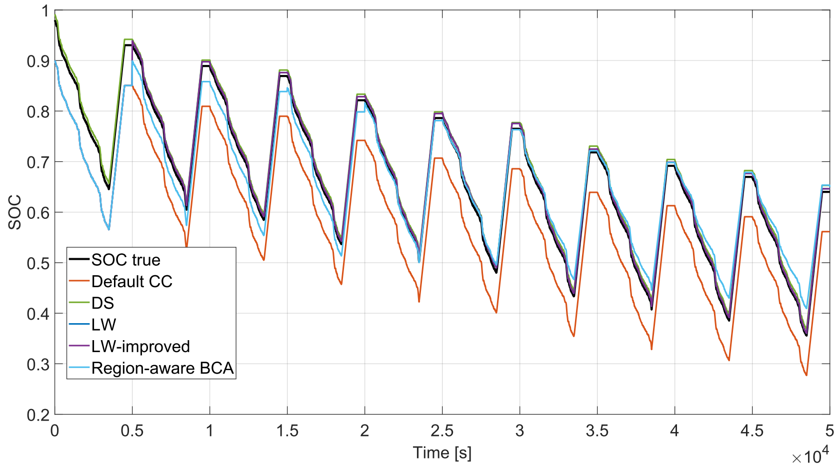

(a) SOC trajectory comparison

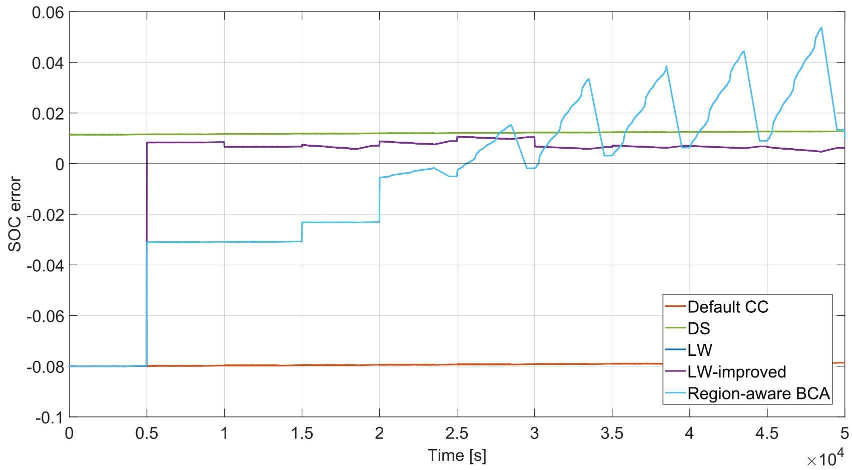

(b) SOC error comparison

Figure 5.1: Representative SOC trajectory and error comparison under initial SOC mismatch, with reference $SOC_0 = 0.98$ and estimator $SOC_0 = 0.90$.

As shown in Figure 5.1, conventional CC preserves the initial offset because no later correction is applied, and the correction methods reduce the SOC error to different extents. The DS-inspired method reduces most of the initial offset at the beginning of the estimation.

5.3.3 Discussion

Case B shows that an initial SOC error mainly behaves as an offset error. For conventional CC, SOC estimation starts from the wrong initial value and follows the same current-integration process as the reference. Without any additional correction, the initial offset is largely preserved during the simulation.

The DS-inspired method is the most directly targeted method for this case because its correction is applied before CC propagation begins. In the first two cases, where the reference initial SOC is 0.98, the LSE-based OCV estimation provides an effective initial SOC correction, so the DS-inspired method greatly reduces the initial offset. However, the case with reference $SOC_0 = 0.80$ and estimator $SOC_0 = 0.90$ shows a clear limitation. In this region, the LFP OCV–SOC curve is flat, so the same level of OCV estimation uncertainty can lead to a much larger SOC ambiguity.

The LW, LW-improved, and BCA methods can also reduce part of the initial offset, but their correction is applied later through cycle-level or slow-state mechanisms rather than by directly recalculating the initial SOC. Therefore, the error reduction is delayed and depends on the availability of valid correction conditions. Particularly, for BCA, the reduction of initial SOC error should not be interpreted as a correct diagnosis of the injected error source. It may reduce the SOC error during later operation through slow-state updates such as effective-capacity adaptation, leading to a smaller error without directly identifying the original error source.

5.4 Case C: Current Measurement Bias

5.4.1 Purpose and Setup

Case C evaluates the influence of systematic current measurement bias on SOC estimation. Since Coulomb Counting integrates the measured current over time, a persistent current offset is expected to produce accumulated SOC drift. Therefore, this case directly examines the sensitivity of each method to propagation error caused by biased current measurement.

Three current bias conditions are considered: $+1$ A, $+0.5$ A and -0.5 A. The two positive biases are used to examine the effect of the bias magnitude, and the negative current bias is set to examine the influence of bias direction.

5.4.2 Results

Table 5.4 shows the error metrics of the cases.

As shown in Table 5.4, conventional CC calculation is strongly influenced by current measurement bias. In all three bias cases, its RMSE exceeds 20%, and the bias sign follows the direction of the injected current offset. This confirms that the current measurement error is time-cumulative. The DS-inspired method does not reduce this drift because its correction is applied only at initialization and does not compensate the biased current during operation. The $+0.5$ A case is selected as a representative example because it shows the same drift mechanism with a moderate bias magnitude. The SOC trajectory and error comparisons are shown in Figure 5.2.

As shown in Figure 5.2, conventional CC gradually deviates from the reference SOC because the biased current accumulates throughout the simulation. The DS-inspired method shows an even larger drift, once again indicating that initialization correction alone cannot compensate for a persistent current-measurement bias. In contrast, the LW, LW-improved, and BCA methods remain much closer to the reference trajectory. This agrees with the quantitative metrics in Table 5.4, where the RMSE under $+0.5$ A drops from 23.18% for conventional CC to below

Table 5.4: SOC estimation error metrics under current-measurement bias

Bias case	Method	RMSE (%)	Bias (%)	MaxAbs (%)
+1 A	Conventional CC	25.10	22.84	41.53
	DS-inspired	31.68	23.22	64.43
	LW	4.74	3.61	10.22
	LW-improved	3.56	-0.46	10.22
	BCA	3.53	2.99	8.77
+0.5 A	Conventional CC	23.18	20.62	37.42
	DS-inspired	27.31	23.83	48.56
	LW	2.65	2.08	5.54
	LW-improved	1.90	0.00	5.54
	BCA	2.13	1.75	5.02
−0.5 A	Conventional CC	27.27	-23.93	42.77
	DS-inspired	27.85	-24.06	49.03
	LW	2.02	-0.72	4.99
	LW-improved	2.34	0.71	4.99
	BCA	1.56	-0.63	4.99

3% for the three correction methods. The time-domain behavior also illustrates the difference between a one-time initial correction and correction during operation.

5.4.3 Discussion

Case C confirms that current measurement bias is one of the most critical error sources for Coulomb Counting. Since the biased current is accumulated at every timestep, the error grows continuously. This behavior explains the large RMSE and MaxAbs values of Conventional CC in all three bias cases.

The DS-inspired method is not designed or reproduced for this type of propagation error. Its correction is applied before CC propagation begins, but the biased current continues to affect SOC update during operation. In comparison, the LW, LW-improved, and BCA methods achieve much lower errors because they include correction mechanisms during operation or at cycle boundaries. The internal reasons for these differences are further examined in Section 5.7.

5.5 Case D: Capacity Mismatch

5.5.1 Purpose and Setup

Case D evaluates the influence of effective-capacity mismatch on SOC estimation. In Coulomb Counting, the SOC change is calculated by scaling the integrated current with the capacity used by the estimator. Therefore, if the actual usable capacity of the battery differs from the estimator capacity, the SOC variation will be incorrectly scaled.

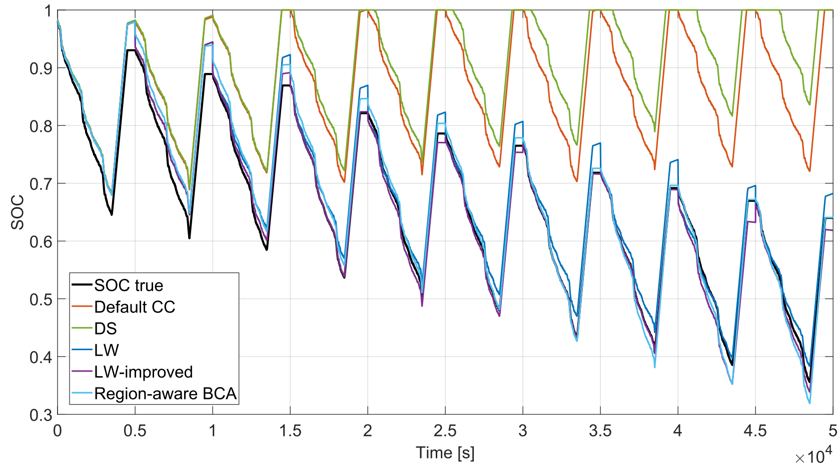

(a) SOC trajectory comparison

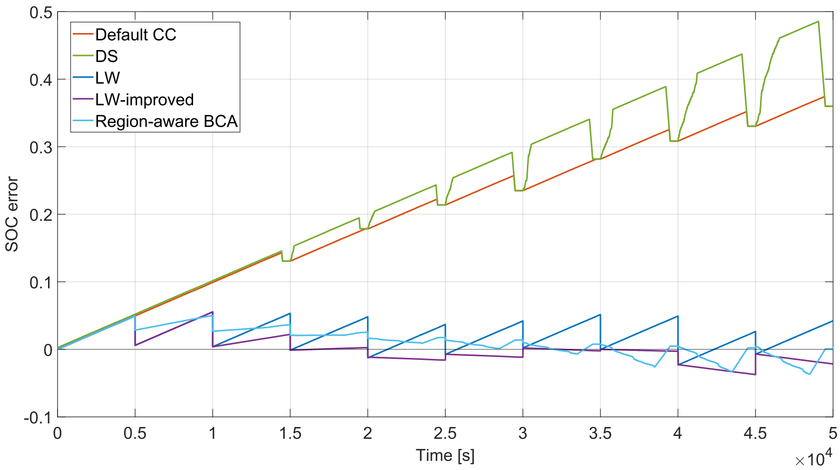

(b) SOC error comparison

Figure 5.2: Representative SOC trajectory and error comparison under +0.5 A current measurement bias.

In this case, the plant capacity is reduced to reflect the capacity loss caused by aging, and the estimator initially uses the nominal capacity. Two capacity factors are used: 0.75 and 0.85 of the nominal capacity, which represent different extents of usable capacity reduction. Capacity increase is not considered because the main battery aging effect is capacity fade.

5.5.2 Results

The results are summarized in Table 5.5.

As listed in Table 5.5, capacity mismatch produces a clear estimation error in conventional

Table 5.5: SOC estimation error metrics under capacity mismatch

Capacity case	**Method**	**RMSE (%)**	**Bias (%)**	**MaxAbs (%)**
Capacity factor = 0.75	Conventional CC	11.59	10.68	21.18
	DS-inspired	12.95	12.14	22.63
	LW	4.59	3.78	11.80
	LW-improved	4.59	3.78	11.80
	BCA	7.00	6.34	13.03
Capacity factor = 0.85	Conventional CC	6.16	5.68	11.22
	DS-inspired	6.90	6.47	12.00
	LW	3.12	2.76	6.71
	LW-improved	3.12	2.76	6.71
	BCA	4.27	3.93	7.63

CC. When the capacity factor is reduced to 0.75 of the nominal value, conventional CC reaches an RMSE of 11.59% and a MaxAbs error of 21.18%. Under the milder capacity factor of 0.85, the error decreases to 6.16%. This indicates that the severity of battery aging will directly affect the SOC scaling error.

The DS-inspired method does not improve performance in this case. The errors are slightly higher than those of conventional CC because the method does not adapt the capacity during estimation. In contrast, the LW and LW-improved methods achieve the lowest errors in both cases. BCA also reduces the error compared with conventional CC, although its improvement is smaller than that of the LW and LW-improved methods.

The capacity factor of 0.75 is selected as the representative case in capacity mismatch. The SOC trajectories and error comparisons are shown in Figure 5.3.

As shown in Figure 5.3, the estimated SOC trajectories remain above the reference SOC under capacity mismatch. This indicates that the estimators underestimate the SOC change produced by a given current input when the capacity used in the estimator is larger than the actual usable capacity.

Figure 5.3b further shows a cycle-dependent error pattern. Within each cycle, the error increases during the driving intervals and partially decreases during charging or standby periods. For methods without capacity update, the error continuously grows. At the same time, for LW, LW-improved and BCA, the same general pattern is still present, but the error magnitude is reduced.

5.5.3 Discussion

The trend in Figure 5.3 is consistent with the nature of capacity mismatch in Coulomb Counting. When the actual usable capacity is lower than the capacity used by the estimator, the denominator in CC calculation is too large. As a result, the SOC changes more slowly than the true trajectory, producing a positive accumulated error.

The results indicate that adaptive capacity update is necessary for this type of error. The

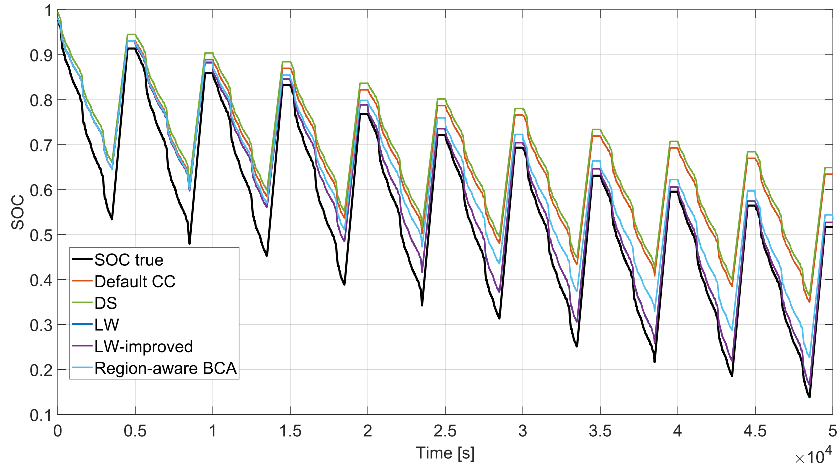

(a) SOC trajectory comparison

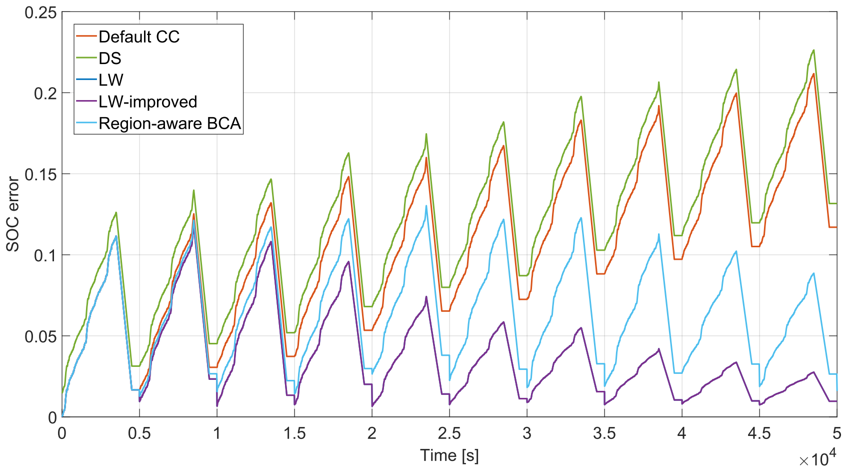

(b) SOC error comparison

Figure 5.3: Representative SOC trajectory and error comparison under capacity mismatch.

LW and LW-improved methods perform best because their cycle-level update directly targets effective-capacity estimation. BCA also reduces the error because effective capacity is included as a slow correction state. However, the error is not fully eliminated because capacity updates depend on reliable correction conditions, such as reliable anchors or endpoint information. If these conditions are not sufficiently informative, a residual SOC error remains.

5.6 Case E: Mixed Error Conditions

5.6.1 Purpose and Setup

Case E evaluates the robustness of the selected methods under mixed-error conditions. Unlike cases B, C, and D, where only one dominant error factor is injected at a time, case E combines two CC-related error sources in each subcase. This is closer to practical operation, where different error sources may coexist.

Three mixed-error cases are considered. The first case combines effective-capacity mismatch with current measurement bias. The second case combines effective-capacity mismatch with initial SOC error. The third case combines initial SOC error with current measurement bias. These cases are used to examine whether different error mechanisms reinforce each other or partially compensate each other.

5.6.2 Results

The error metrics under mixed error sources are listed in Table 5.6.

Table 5.6: SOC estimation error metrics under mixed error conditions

Mixed case	**Method**	**RMSE (%)**	**Bias (%)**	**MaxAbs (%)**
$0.85Q_n$ & 1 A	Conventional CC	31.05	28.47	51.11
	DS-inspired	37.27	28.86	75.90
	LW	7.71	6.79	12.81
	LW-improved	4.54	3.09	12.81
	BCA	6.03	5.16	12.93
$0.85Q_n$ & $SOC_0 = 0.90$	Conventional CC	3.34	-2.32	8.00
	DS-inspired	6.90	6.47	12.00
	LW	3.39	1.96	8.00
	LW-improved	3.39	1.96	8.00
	BCA	4.72	2.72	10.04
$SOC_0 = 0.90$ & 0.5 A	Conventional CC	21.22	16.28	37.42
	DS-inspired	27.31	23.83	48.56
	LW	3.07	1.27	8.00
	LW-improved	2.60	-0.51	8.00
	BCA	2.19	0.55	8.00

As shown in Table 5.6, mixed-error conditions can produce larger errors than the corresponding single-error cases when the error sources reinforce each other. In the case of combining capacity mismatch and $+1$ A current bias, conventional CC reaches an RMSE of 31.05%, while the DS-inspired method reaches an RMSE of 37.27% and a MaxAbs error of 75.90%.

Mixed case 2, however, shows a different behavior. All the methods achieve a relatively low error extent. Although conventional CC gives a relatively low RMSE of 3.34%, this should not be interpreted as true robustness. In this scenario, the effects of the initial SOC offset and the capacity degradation produce errors in opposite directions, so the net SOC error is partly reduced due to error cancelation.

Mixed case 1, which combines the capacity factor 0.85 with +1 A current bias, is selected as the representative mixed-error example. Figure 5.4 shows the SOC trajectory and SOC error comparisons for this case.

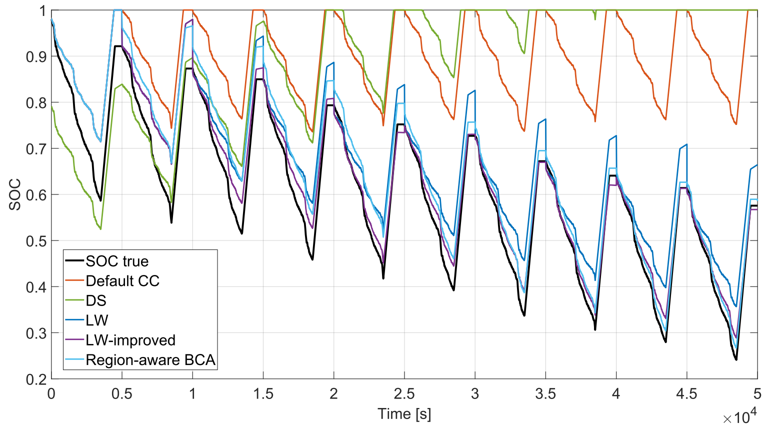

(a) SOC trajectory comparison

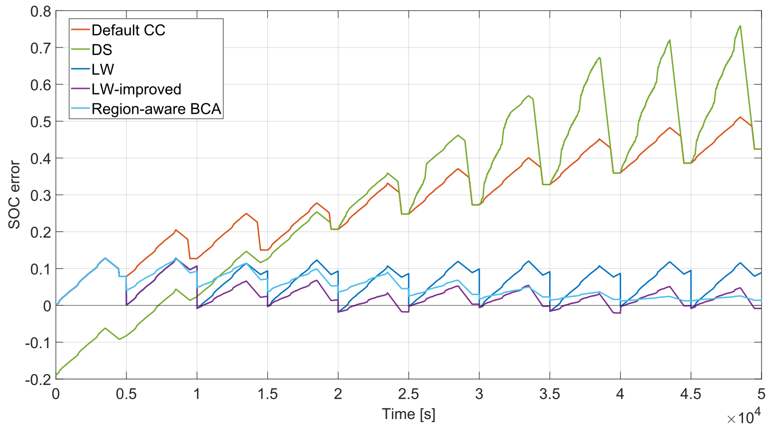

(b) SOC error comparison

Figure 5.4: Representative SOC trajectory and error comparison for mixed case 1: capacity factor 0.85 with +1 A current bias.

Figure 5.4 shows that conventional CC and the DS-inspired method gradually drift away from the reference SOC, and the SOC errors develop a growing positive baseline over repeated cycles.

The LW, LW-improved, and BCA methods show smaller error growth. Their trajectories still contain cycle-dependent fluctuations, but the accumulated error is more bounded. Among these methods, the LW-improved method gives the lowest RMSE, and BCA provides a comparable but slightly more conservative result.

5.6.3 Discussion

Case E shows that mixed SOC estimation errors are not necessarily additive in a simple way. Depending on their signs and how they interact with the operating profile, different error sources may either reinforce or partially compensate for each other. Mixed case 1 illustrates a reinforcing situation in which current measurement bias and capacity mismatch both contribute to accumulated propagation error. As a result, conventional CC and the DS-inspired method show large deviations.

Mixed case 2 shows the opposite situation. Although the numerical error is relatively small for several methods, this should not be interpreted as true robustness. In this case, the initial SOC offset and the capacity mismatch partially cancel each other, leading to a lower net SOC error. Therefore, mixed-error cases should be interpreted together with the corresponding single-error cases and, when available, method-specific diagnostic indicators.

5.7 Method-Specific Diagnostic

The previous sections evaluated the SOC estimation methods from a case-based perspective. The tables and trajectory comparisons show the external estimation performance, but they do not fully explain how each method produces its correction. Therefore, this section examines selected method-specific diagnostic variables. The purpose is to connect the observed case-level performance with the internal correction mechanisms of the methods.

Because the selected methods use different correction principles, their diagnostic variables are also different. For the DS-inspired method, the relevant diagnostics are the OCV estimation and initial SOC inversion. For the LW-based methods, the relevant diagnostics are the capacity update, voltage-anchor reset, and current-bias estimate. For BCA, the relevant diagnostics are the slow-state updates and the voltage-observability gate.

5.7.1 DS-Inspired Method: OCV-Based Initial SOC Diagnostic

The DS-inspired method is mainly an initialization-oriented correction method. Unlike other selected algorithms, it does not continuously estimate parameters during operation. Instead, it estimates an OCV-related quantity from voltage-current data using a first-order RC least-squares approximation, and then maps the estimated OCV to SOC through the OCV–SOC lookup table. As a result, the most relevant diagnostics for this method are the OCV fitting result and the initial SOC inversion.

Two diagnostic cases are selected to illustrate the behavior. The first case shows effective correction when the initial SOC error occurs in a region with useful OCV–SOC information. The second case shows limited correction when the SOC lies in a flatter LFP voltage region, where OCV–SOC inversion becomes less reliable.

Figure 5.5 shows the diagnostic result for the case with reference $SOC = 0.98$ and estimator $SOC = 0.85$. The upper plot compares the LSE-estimated OCV with the fitted OCV model, while the lower plot shows the OCV–SOC inversion used to obtain the corrected initial SOC.

In this case, the estimated OCV leads to an initial SOC close to the reference condition, which explains the strong improvement of the DS-inspired method in the initial SOC error cases.

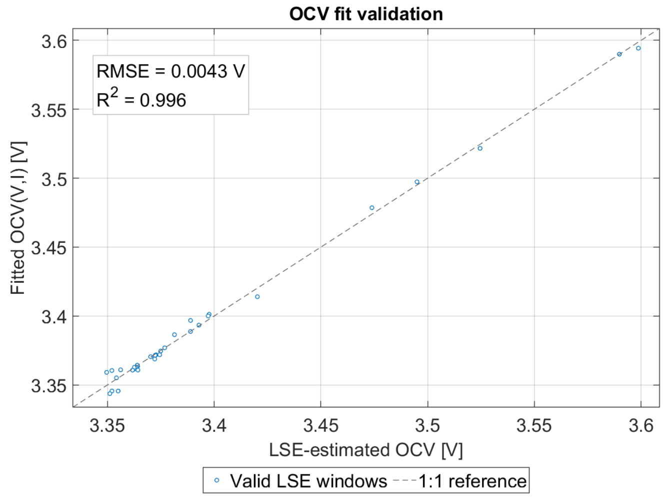

(a) OCV fitting validation using valid LSE windows.

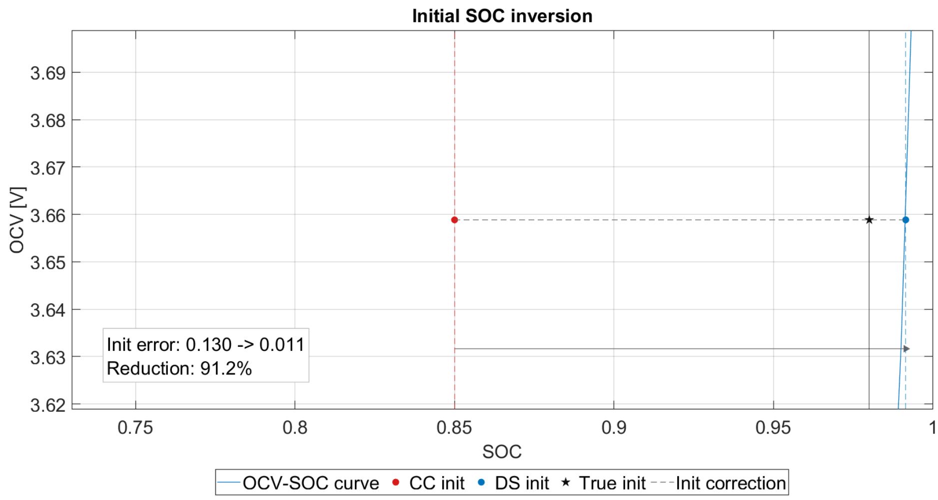

(b) Initial SOC inversion through the OCV–SOC lookup table.

Figure 5.5: DS-inspired initial SOC correction in the Ref. $SOC_0 = 0.98$, est. $SOC_0 = 0.85$ case. The fitted OCV model agrees well with the valid LSE-estimated OCV samples.

Figure 5.6 shows a case where the DS-inspired correction is more limited. Although the same OCV-based initialization procedure is applied, the resulting SOC correction does not fully remove the initial offset. This is consistent with the weak voltage observability of LFP cells in the plateau region. Even when the LSE step provides a smoother OCV estimate than a single voltage sample, the final SOC correction still depends on OCV–SOC inversion. In the flat plateau region, a small OCV uncertainty can correspond to a large SOC ambiguity.

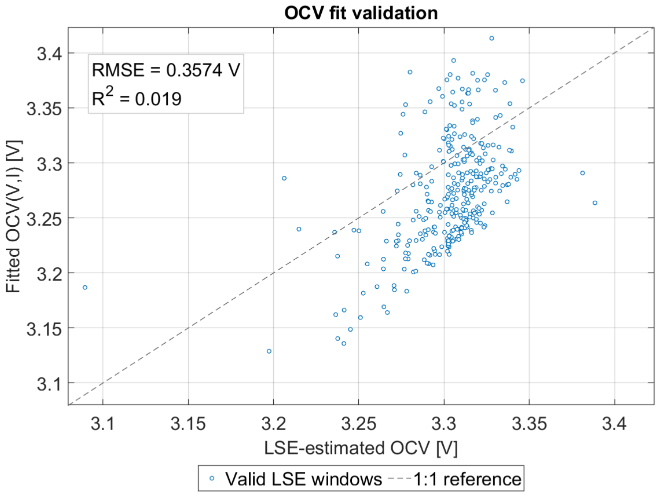

(a) OCV fit validation of the DS-inspired method.

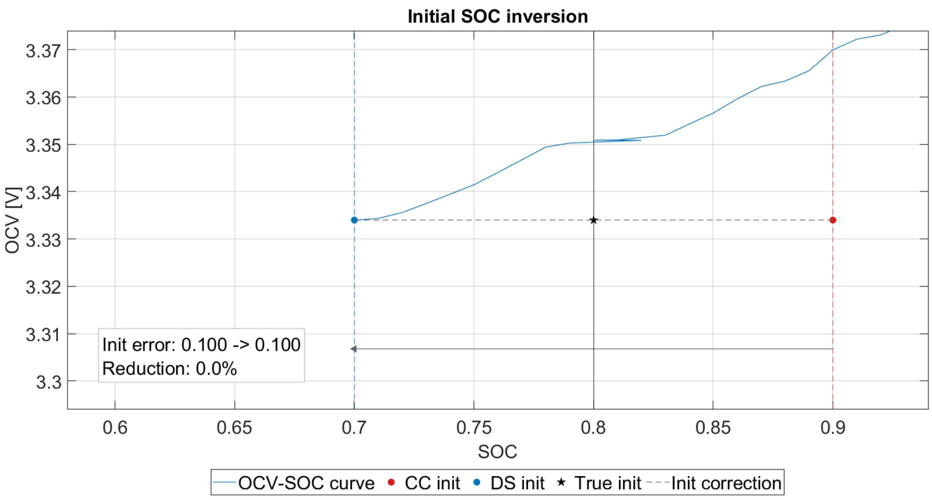

(b) Initial SOC inversion

Figure 5.6: DS-inspired diagnostic for the limited correction case. The OCV fit has weak agreement with the LSE-estimated OCV, and the resulting initial SOC inversion does not reduce the initial SOC error.

These diagnostics explain the DS-inspired trends observed in the case-based results. The method performs well when the dominant error is an initial SOC offset and the OCV–SOC mapping is sufficiently informative. However, it is less effective when the SOC lies in a weakly observable plateau region or when the dominant error appears during propagation, such as current-measurement bias or capacity mismatch.

5.7.2 LW and LW-Improved Methods: Capacity and Bias Diagnostics

The LW and LW-improved methods share the same cycle-level correction structure. Both methods use cycle-level information to update correction parameters and apply SOC reset. Therefore, the relevant diagnostics are the effective-capacity update, the activation of update gates, and the additional current bias estimation of the LW-improved method.

For the original LW method, the most relevant diagnostic is the effective-capacity update. Figure 5.7 shows the capacity update behavior under the capacity mismatch case with the plant capacity scaled to 0.75 of the nominal value. The upper plot shows the capacity used in the Coulomb Counting update; the middle figure shows the capacity candidate value before acceptance, and the lower figure shows whether the update gate is active. The gate remains inactive during the first two cycles and becomes active from the third cycle onward, after the validity conditions are satisfied.

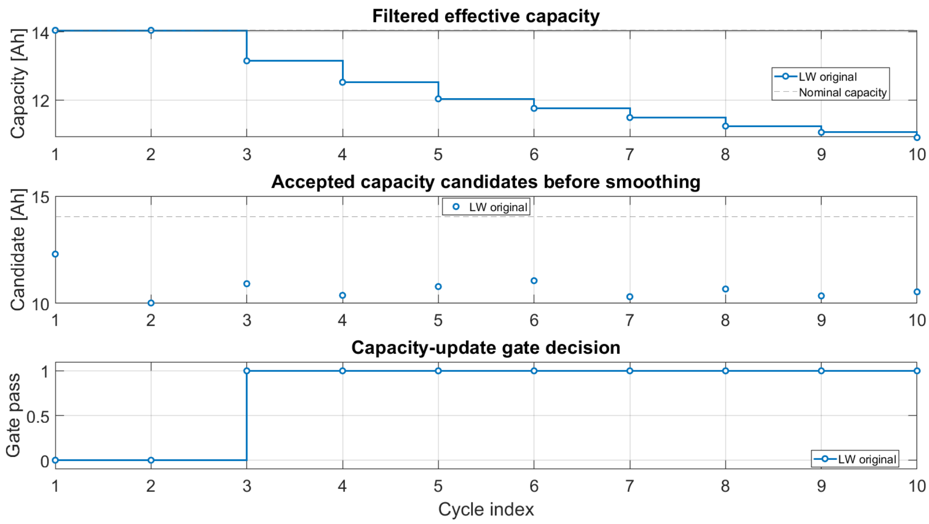

Figure 5.7: Capacity update diagnostics of the original LW method under the capacity mismatch case with the plant capacity scaled to 0.75 of the nominal value.

The LW-improved method keeps the same capacity-update structure but adds a cycle-level current bias detector. Figure 5.8 shows the raw bias estimate, the filtered bias estimate, and the bias-update gate under the negative current-bias case. The raw estimate is only accepted when it is sufficiently persistent and consistent across cycles.

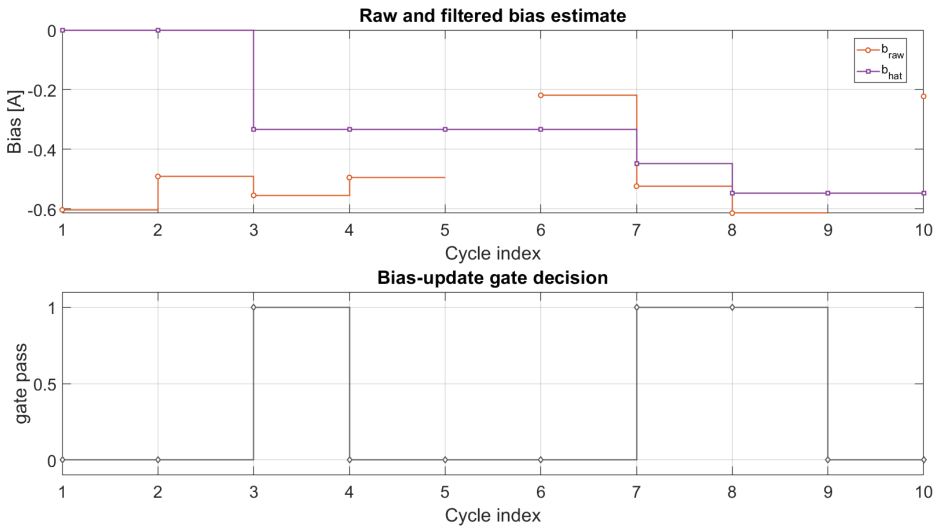

Figure 5.8: Bias update diagnostics of the LW-improved method under the negative current drift case. The raw cycle-level bias estimate is accepted only when the gate condition is satisfied, allowing the filtered estimate to gradually approach the injected current bias.

Together, these diagnostics show that the original LW method mainly improves SOC estimation through cycle-level capacity update and voltage-anchor reset, while the LW-improved method extends the same framework with guarded current-bias correction. This explains why both methods perform well under capacity mismatch, and why LW-improved provides additional benefit when persistent current-measurement bias is present.

5.7.3 BCA Method: Slow-State and Voltage-Observability Diagnostics

The BCA method is designed to reduce dependence on voltage-based SOC correction. Its diagnostics focus on two aspects: the slow-state updates for current bias and effective capacity, and the voltage-observability gate that decides whether voltage anchor is allowed. Figure 5.9 shows the BCA response under the $-0.5\ A$ current bias case. The upper plot shows the SOC error and uncertainty band, and the lower plot shows the slow-state adaptation to current bias and effective capacity.

As shown in Figure 5.9a, the SOC error remains much closer to zero after the slow correction states are updated. The estimated current bias gradually approaches the injected bias of approximately -0.5 A, while the effective capacity also changes during the same cycles. This indicates that BCA reduces current drift mainly through slow-state correction rather than through direct voltage reset. The simultaneous change in effective capacity also shows that the slow states are coupled, which helps explain the later variation in the SOC error.

A second diagnostic is used to illustrate the optional voltage anchor. Figure 5.10 shows the BCA behavior under the case with reference $SOC_0 = 0.80$ and estimator $SOC_0 = 0.90$.

As shown in Figure 5.10, BCA-CC applies voltage anchoring only when the local OCV–SOC slope is sufficiently informative. The voltage anchor gain α_V increases in observable regions,

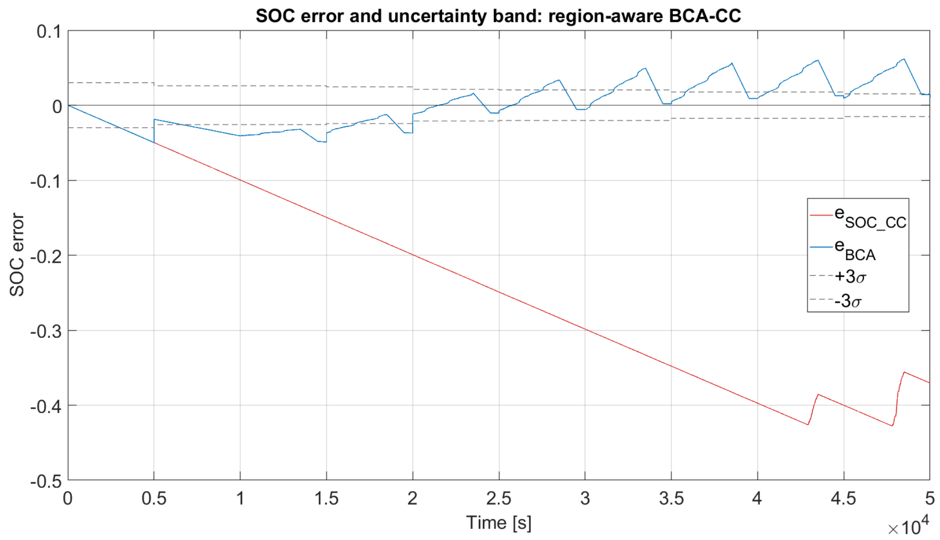

(a) SOC error and uncertainty band.

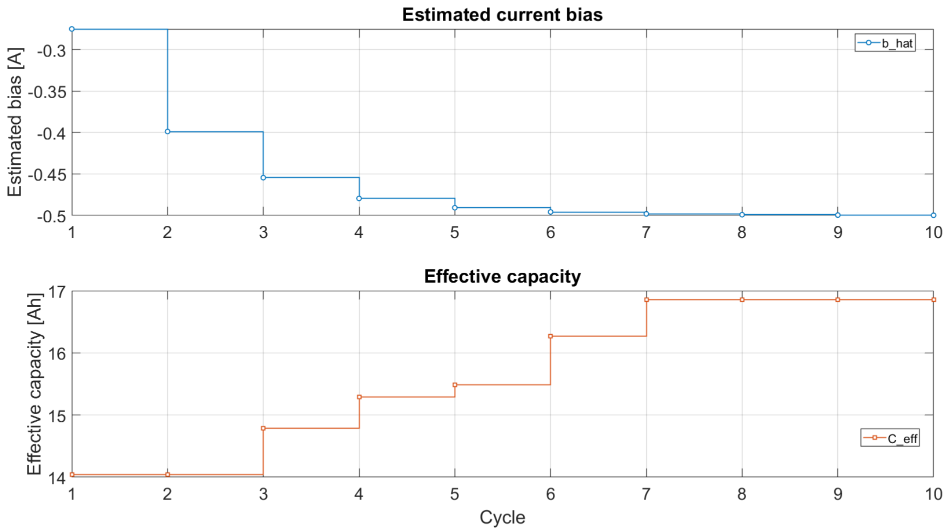

(b) Slow-state adaptation.

Figure 5.9: BCA under the negative current drift case. The current-bias estimate converges towards the injected bias, while the effective-capacity update acts as a secondary coupled state and affects the later SOC error evolution.

while the applied correction $\Delta SOC_{\text{anchor}}$ remains bounded. This behavior is consistent with the design intention of BCA, where voltage information is not discarded but is only used as an optional and supplementary correction source.

Overall, the diagnostic results provide a mechanism-level explanation for the performance

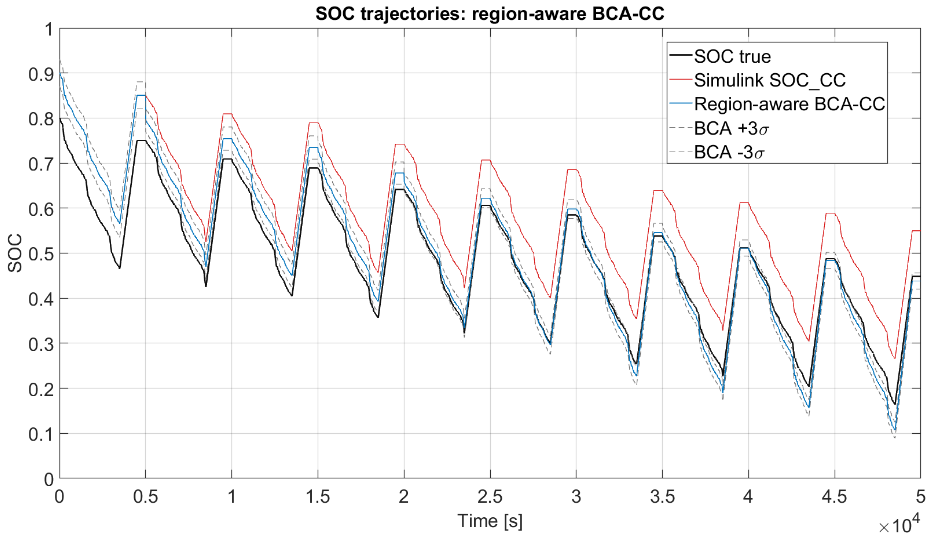

(a) SOC trajectories.

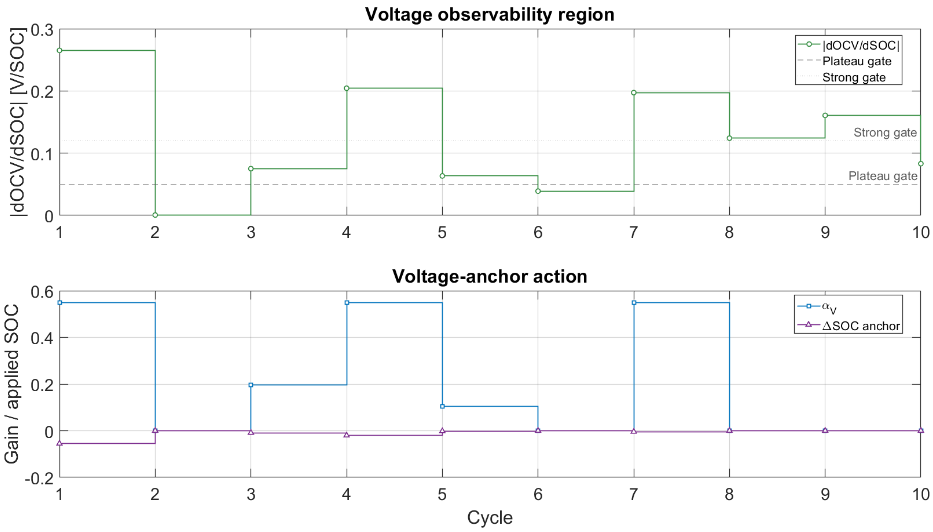

(b) Voltage observability and anchor action.

Figure 5.10: BCA diagnostics under the SOC-higher case. The voltage-anchor gain is increased only in regions where the OCV–SOC slope provides sufficient voltage observability, while the applied SOC correction remains bounded.

trends. The DS-inspired method is mainly limited by the reliability of OCV–SOC inversion, the LW-based methods depend on valid cycle-level updates and anchor conditions, and BCA depends on the activation of slow-state correction and voltage-observability gates.

5.8 Summary

This chapter evaluated the SOC estimation methods under baseline, initial-SOC, current-bias, capacity-mismatch, and mixed-error conditions. The case-based results show that the relative performance of each method strongly depends on the dominant error source. As summarized in Figure 5.11, no single correction mechanism performs best in all cases.

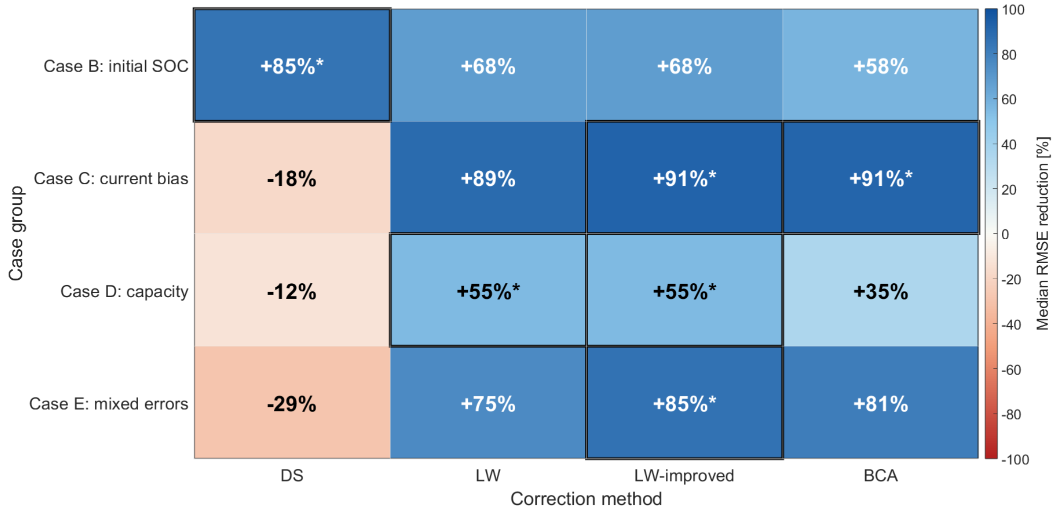

Figure 5.11: Grouped SOC RMSE reduction relative to the conventional CC baseline. Positive values indicate improvement, and boxed cells mark the best median performance within each error group.

The grouped results indicate that each error type favors a different correction mechanism. The DS-inspired method performs best when the dominant error is an incorrect initial SOC and when a reliable OCV fit can be obtained outside the OCV plateau region. The LW method performs well under capacity mismatch because its cycle-level update directly targets the dominant error source. The LW-improved method retains the capacity update structure and adds guarded current-bias compensation, which improves its performance under current-bias and mixed-error conditions. The BCA method provides a primarily current-driven correction structure with slow-state adaptation and optional voltage anchoring. It can reduce current-bias and capacity-related errors, but its performance depends on the availability of valid standby, capacity-update, and voltage-observability conditions.

Overall, the results confirm that CC-based SOC correction should be selected according to the dominant error mechanism. Initial SOC error, current-measurement bias, and capacity mismatch require different correction mechanisms, and the reliability of each correction also depends on the available observability and validity conditions.

Chapter 6

Conclusion and Future Work

6.1 Main Conclusions

This thesis investigates selected CC-based SOC correction methods from the perspective of future BMS development for LFP-based heavy-duty battery systems. The main challenge is not only to improve conventional Coulomb Counting, but also to determine which part of the SOC error can be corrected under the available operating conditions. The results show that CC correction should be decomposed according to the underlying error mechanisms, such as initial SOC error, current-measurement bias, and capacity mismatch. At the same time, each correction strategy must be constrained by the observability and reliability of the signals used in the correction.

A key conclusion is that the LFP voltage plateau affects more than the accuracy of OCV-based SOC lookup. It also narrows the usable correction bandwidth of the whole estimator. Initial SOC correction, cycle-level anchoring, and capacity adaptation all become less certain when the voltage signal does not provide a strong SOC reference. This means that voltage information should not be treated as a continuously reliable SOC anchor for LFP cells. Instead, it should be used as a conditional correction signal, depending on the SOC region, relaxation condition, and local OCV–SOC slope.

Another conclusion is that peak accuracy in an isolated case and robustness across cases are different design objectives. A method may achieve the lowest error when its assumptions match a specific injected error, but the same assumptions may become invalid when the operating conditions or error combinations change. Therefore, the most useful estimator is not necessarily the one that gives the best RMSE in one case, but the one whose correction mechanisms can identify when their supporting evidence is trustworthy and when correction should remain conservative.

Overall, CC remains a suitable propagation core because it is simple, efficient, and accurate over short periods when its assumptions are satisfied. However, it should not be used as an unguarded standalone estimator in LFP-based HDV applications. Current-bias compensation, capacity adaptation, and voltage anchoring should be activated only when their diagnostic evidence is sufficiently reliable. In this sense, the main conclusion of the thesis is that correction strength should be limited by correction reliability.

6.2 Answers to Research Questions

6.2.1 RQ1

How can an existing Simulink battery example be adapted into a unified benchmark for evaluating CC-based SOC estimation and enhancement methods for LFP batteries under dynamic heavy-duty operating conditions?

The original MathWorks BMS example was adapted into a benchmark focusing on SOC estimation by modifying battery model, operating scenario, and error case injection. The battery model was parameterized for an LFP cell, and the operating profile was reorganized into a repeated HDV-oriented cycle consisting of driving, charging, and standby stages.

Controlled error cases were then introduced based on the main error sources of Coulomb Counting, including current-measurement bias, initial SOC error, effective-capacity mismatch, and mixed-error combinations. All evaluated methods were implemented under the same battery model, operating profile, SOC error definition, and performance metrics. Therefore, the benchmark provides a controlled and repeatable platform for comparing CC-based SOC correction strategies under representative LFP/HDV conditions.

From a company BMS development perspective, the benchmark can also serve as an early-stage screening platform before experimental validation and embedded implementation.

6.2.2 RQ2

How do the selected CC-based enhancement methods perform compared with basic Coulomb Counting under the same battery model, operating profile, error scenarios, and evaluation metrics?

The results show that the selected CC-based correction methods do not uniformly outperform basic CC under all conditions. In the baseline case, basic CC gives the lowest error because its assumptions are satisfied, and no correction is required. However, when propagation errors are introduced, especially current measurement bias and capacity mismatch, basic CC accumulates clear SOC drift because it has no self-correction mechanism.

The improvement of each correction method depends on the dominant error source. The DS-inspired method is most effective for initial SOC error when the local OCV–SOC slope is sufficiently large. The LW method performs well under capacity mismatch because its cycle-level capacity update targets the dominant scaling error. The LW-improved method improves current-bias and mixed-error cases through guarded bias compensation. The BCA method also reduces current-bias and capacity-related errors through slow-state adaptation and region-aware voltage anchoring, but its correction is more conservative.

The mixed-error cases further show that different error sources can reinforce or partially compensate each other, so a low error in one mixed case does not necessarily indicate general robustness. Overall, the selected CC enhancement methods improve basic CC only when the correction mechanism matches the dominant error source and the correction signal is sufficiently observable.

6.2.3 RQ3

What are the advantages, limitations, and applicable conditions of these methods for LFP-based heavy-duty battery management systems?

The applicability of each method depends on whether the signals required by its correction mechanism are observable and reliable during operation. Basic CC is suitable as a low-complexity propagation core, but it cannot correct accumulated errors by itself. The DS-inspired method is useful for initial SOC correction when a stable and informative OCV estimate is available, but it is limited in the flat LFP plateau and is not suitable as a general online correction mechanism.

The LW method is useful when reliable cycle boundaries and voltage anchors are available, especially under effective-capacity mismatch. However, its cycle-level update can be affected by current bias and weak voltage observability. The LW-improved method addresses part of this limitation by adding guarded current-bias compensation, but it still depends on valid cycle segmentation and consistent bias evidence.

The developed BCA method is more conservative and reduces dependence on voltage-derived SOC correction. It uses rest-window evidence for current-bias estimation, slow effective-capacity adaptation, and voltage anchoring only when the local OCV–SOC slope is sufficiently informative. Its limitation is that the slow correction states are not fully independent, and it does not always give the lowest RMSE. Overall, for LFP-based HDV BMS development, the SOC estimator should be designed as a guarded CC-based architecture rather than as a single fixed correction rule.

6.3 Future Work

The benchmark developed in this thesis provides a controlled basis for comparing SOC correction methods according to their dominant error mechanisms. Future work should therefore focus on validating this benchmark with experimental data and extending it to more realistic operating conditions and more advanced estimator structures.

First, the evaluated methods should be validated using experimental LFP battery data. The present study is based on a Simulink benchmark, which provides a repeatable comparison environment, but real measurements may affect the correction mechanisms through voltage noise, current-sensor offset, relaxation behavior, and temperature variation. In particular, future experiments should verify whether the limited DS performance in the LFP plateau remains under real voltage noise and relaxation behavior, whether the LW and LW-improved update gates remain stable with measured current and voltage signals, and whether the BCA method can detect reliable standby windows when current measurement contains noise and offset. Recent rest-window-based LFP SOC estimation studies also show that short-term rest measurements can be useful for improving Coulomb Counting initialization, which supports further experimental investigation of this direction [43].

Second, the benchmark should be extended to more realistic and irregular HDV operating profiles. The operating scenario is organized into repeated driving, charging, and standby stages. This structure is useful for controlled comparison, but real vehicles may have irregular rest periods, varying load intensity, and changing ambient conditions. Since several correction mechanisms rely on valid rest windows, cycle boundaries, or update gates, future work should test whether these conditions can be detected reliably in less regular operating conditions.

Third, the interaction between current bias estimation and capacity adaptation should be further studied. In the BCA method, the corrected current affects the estimation of amount of charge, while the effective capacity influences the response to that amount. As a result, an imperfect update in one slow state may affect the other. Future work should develop a more explicit decoupling strategy, such as separating bias estimation and capacity estimation over different time scales or by adding stronger consistency checks before accepting capacity updates.

Fourth, future work should examine how short-term capacity correction can be distinguished from long-term aging estimation. In the thesis, capacity mismatch is represented using fixed capacity factors, and the adaptive methods are used to reduce the SOC scaling error. However, in real operation, apparent capacity error may arise from battery aging, ambient temperature, or incomplete relaxation. Therefore, a future framework should be able to identify whether the observed capacity trend is stable enough to be interpreted as SOH-related degradation. This direction is related to recent studies on online SOC and capacity co-estimation under different aging states [44].

Finally, the benchmark can be extended beyond CC-based correction methods to model-based and hybrid SOC estimators. Recent LFP SOC studies have proposed robust, bias-compensated, information-aware, and adaptive model-based strategies to address the flat OCV–SOC plateau, measurement bias, and limited voltage observability [22, 23, 25, 45]. Extending the same LFP/HDV benchmark to methods such as EKF, UKF, or hybrid model-based estimators would help clarify the trade-off between accuracy, robustness, computational cost, and computational effort under the same error scenarios. This would further support the embedded BMS algorithm selection for LFP-based heavy-duty battery systems.

Bibliography

[1] European Automobile Manufacturers' Association (ACEA), "CO_2 Standards for Heavy-Duty Vehicles: Fact Sheet," https://www.acea.auto/files/Fact-sheet-CO2_standards_for_heavy_duty_vehicles.pdf, 2023.

[2] European Parliament and the Council of the European Union, "Regulation (EU) 2024/1610 of the European Parliament and of the Council of 14 May 2024," 2024.

[3] G. Giuliano, M. Dessouky, S. Dexter, J. Fang, S. Hu, and M. Miller, "Heavy-Duty Trucks: The Challenge of Getting to Zero," *Transportation Research Part D: Transport and Environment*, vol. 93, p. 102742, Apr. 2021.

[4] W. Shoman, S. Yeh, F. Sprei, P. Plötz, and D. Speth, "Battery Electric Long-Haul Trucks in Europe: Public Charging, Energy, and Power Requirements," *Transportation Research Part D: Transport and Environment*, vol. 121, p. 103825, Aug. 2023.

[5] B. Borlaug, M. Muratori, M. Gilleran, D. Woody, W. Muston, T. Canada, A. Ingram, H. Gresham, and C. McQueen, "Heavy-Duty Truck Electrification and the Impacts of Depot Charging on Electricity Distribution Systems," *Nature Energy*, vol. 6, no. 6, pp. 673–682, Jun. 2021.

[6] D. Andrea, *Battery Management Systems for Large Lithium-Ion Battery Packs*. Artech House, 2010.

[7] W. Waag, C. Fleischer, and D. U. Sauer, "Critical Review of the Methods for Monitoring of Lithium-Ion Batteries in Electric and Hybrid Vehicles," *Journal of Power Sources*, vol. 258, pp. 321–339, Jul. 2014.

[8] L. Lu, X. Han, J. Li, J. Hua, and M. Ouyang, "A review on the key issues for lithium-ion battery management in electric vehicles," *Journal of Power Sources*, vol. 226, pp. 272–288, Mar. 2013.

[9] K. Liu, K. Li, Q. Peng, and C. Zhang, "A Brief Review on Key Technologies in the Battery Management System of Electric Vehicles," *Frontiers of Mechanical Engineering*, vol. 14, no. 1, pp. 47–64, Mar. 2019.

[10] Y. Xing, E. W. M. Ma, K. L. Tsui, and M. Pecht, “Battery Management Systems in Electric and Hybrid Vehicles,” *Energies*, vol. 4, no. 11, pp. 1840–1857, Nov. 2011.

[11] M. Daowd, N. Omar, P. Van Den Bossche, and J. Van Mierlo, “Passive and active battery balancing comparison based on MATLAB simulation,” in *2011 IEEE Vehicle Power and Propulsion Conference*, 2011, pp. 1–7.

[12] A. Kurkin, A. Chivenkov, D. Aleshin, I. Trofimov, A. Shalukho, and D. Vilkov, “Battery Management System for Electric Vehicles: Comprehensive Review of Circuitry Configuration and Algorithms,” *World Electric Vehicle Journal*, vol. 16, no. 8, p. 451, Aug. 2025.

[13] A. O. Ali, O. Abdelrehim, M. M. Saafan, M. R. Elmarghany, and A. M. Hamed, “Comprehensive Review of Battery Management Systems for Electric Vehicles: Thermal Management, Charging Strategies, and Emerging Technologies,” *Journal of Power Sources*, vol. 658, p. 238269, Dec. 2025.

[14] R. Xiong, *Battery Management Algorithm for Electric Vehicles*. Singapore: Springer Singapore, 2020.

[15] R. Xiong, J. Cao, Q. Yu, H. He, and F. Sun, “Critical Review on the Battery State of Charge Estimation Methods for Electric Vehicles,” *IEEE Access*, vol. 6, pp. 1832–1843, 2018.

[16] M. T. Mumtaz Noreen, M. H. Fouladfar, and N. Saeed, “Evaluation of Battery Management Systems for Electric Vehicles Using Traditional and Modern Estimation Methods,” *Network*, vol. 4, no. 4, pp. 586–608, Dec. 2024.

[17] International Energy Agency, “Electric vehicle batteries,” Global EV Outlook 2025, 2025.

[18] International Renewable Energy Agency, “Critical materials: Batteries for electric vehicles,” International Renewable Energy Agency, Tech. Rep., 2024.

[19] Faraday Institution, “Developments in lithium-ion battery cathodes,” Faraday Institution, Tech. Rep. Faraday Insights 18, 2023.

[20] S. Evro, A. Ajumobi, D. Mayon, and O. S. Tomomewo, “Navigating Battery Choices: A Comparative Study of Lithium Iron Phosphate and Nickel Manganese Cobalt Battery Technologies,” *Future Batteries*, vol. 4, p. 100007, 2024.

[21] D. Jöst, L. N. Palaniswamy, K. L. Quade, and D. U. Sauer, “Towards Robust State Estimation for LFP Batteries: Model-in-the-loop Analysis with Hysteresis Modelling and Perspectives for Other Chemistries,” *Journal of Energy Storage*, vol. 92, p. 112042, Jul. 2024.

[22] J. Shi, S. Jiang, S. Tao, J. Lee, M. Borah, and S. Moura, “An Adaptive Estimation Approach based on Fisher Information to Overcome the Challenges of LFP Battery SOC Estimation,” Jul. 2025.

[23] K. Zhang, C. Chen, L. Er, W. Shen, and R. Xiong, “Robust State-of-Charge Estimation for $LiFePO_4$ Lithium-ion Batteries with Pronounced Voltage Plateau Regions,” *Applied Energy*, vol. 401, p. 126755, 2025.

[24] J. Dambrowski, “Review on Methods of State-of-Charge Estimation with Viewpoint to the Modern LiFePO4/Li4Ti5O12 Lithium-Ion Systems,” in *INTELEC 2013 – The 35th International Telecommunications Energy Conference*, Hamburg, Germany, Oct. 2013.

[25] D. Paizulamu, L. Cheng, Y. Zhuang, H. Xu, N. Qi, and S. Ci, “LiFePO4 Battery SOC Estimation under OCV-SOC Curve Error Based onAdaptive Multi-Model Kalman Filter,” Oct. 2024.

[26] Orion BMS, “State of charge calculation with dynamic drift,” https://www.orionbms.com/features/state-of-charge-with-drift/, accessed: 2026-07-07.

[27] Victron Energy, “Smartshunt manual: Operation,” https://www.victronenergy.com/media/pg/SmartShunt/en/operation.html, accessed: 2026-07-07.

[28] Texas Instruments, “Choosing between battery gas gauges and battery monitors,” https://www.ti.com/lit/SLUA358, accessed: 2026-07-07.

[29] K. Movassagh, S. A. Raihan, and B. Balasingam, “Performance Analysis of Coulomb Counting Approach for State of Charge Estimation,” in *2019 IEEE Electrical Power and Energy Conference (EPEC)*, 2019, pp. 1–6.

[30] S. Das, S. Samanta, and S. Gupta, “Online state-of-charge estimation by modified coulomb counting method based on the estimated parameters of lithium-ion battery,” *International Journal of Circuit Theory and Applications*, vol. 52, no. 2, pp. 749–768, 2024.

[31] J. Lee and J. Won, “Enhanced Coulomb Counting Method for SoC and SoH Estimation Based on Coulombic Efficiency,” *IEEE Access*, vol. PP, pp. 1–1, Jan. 2023.

[32] O. Demirci, S. Taskin, E. Schaltz, and B. Acar Demirci, “Review of Battery State Estimation Methods for Electric Vehicles - Part I: SOC Estimation,” *Journal of Energy Storage*, vol. 87, p. 111435, May 2024.

[33] H. Liu, Z. Wei, W. He, and J. Zhao, “Thermal issues about Li-ion batteries and recent progress in battery thermal management systems: A review,” *Energy Conversion and Management*, vol. 150, pp. 304–330, Oct. 2017.

[34] Y. Xing, W. He, M. Pecht, and K. L. Tsui, “State of Charge Estimation of Lithium-Ion Batteries Using the Open-Circuit Voltage at Various Ambient Temperatures,” *Applied Energy*, vol. 113, pp. 106–115, Jan. 2014.

[35] B. Yi, X. Du, J. Zhang, X. Wu, Q. Hu, W. Jiang, X. Hu, and Z. Song, “Bias-Compensated State of Charge and State of Health Joint Estimation for Lithium Iron Phosphate Batteries,” *IEEE Transactions on Power Electronics*, vol. 40, no. 2, pp. 3033–3042, Feb. 2025.

[36] C. S. Huang, “A Lithium-Ion Batteries Fault Diagnosis Method for Accurate Coulomb Counting State-of-Charge Estimation,” *Journal of Electrical Engineering and Technology*, vol. 19, no. 1, pp. 433–442, Jan. 2024.

[37] P. Shrivastava, T. K. Soon, M. Y. I. B. Idris, and S. Mekhilef, “Overview of Model-Based Online State-of-Charge Estimation Using Kalman Filter Family for Lithium-Ion Batteries,” *Renewable and Sustainable Energy Reviews*, vol. 113, p. 109233, Oct. 2019.

[38] G. L. Plett, “Extended Kalman filtering for battery management systems of LiPB-based HEV battery packs: Part 3. State and parameter estimation,” *Journal of Power Sources*, vol. 134, no. 2, pp. 277–292, Aug. 2004.

[39] P. Eleftheriadis, S. Giazitzis, S. Leva, and E. Ogliari, “Data-Driven Methods for the State of Charge Estimation of Lithium-Ion Batteries: An Overview,” *Forecasting*, vol. 5, no. 3, pp. 576–599, Sep. 2023.

[40] H. Sorouri, A. Oshnoei, M. Marinescu, and R. Teodorescu, “Physics-Informed Multi-Head Attention-Based SOC Estimation for LFP Batteries Using Only Measured Signals,” *IEEE Access*, vol. 14, pp. 65 586–65 599, 2026.

[41] K. Movassagh, A. Raihan, B. Balasingam, and K. Pattipati, “A Critical Look at Coulomb Counting Approach for State of Charge Estimation in Batteries,” *Energies*, vol. 14, no. 14, Jul. 2021.

[42] MathWorks, “Battery Management System Demo,” 2022, MATLAB/Simulink R2022b reference demo model.

[43] Y. Che, L. Xu, R. Teodorescu, X. Hu, and S. Onori, “Enhanced SOC Estimation for LFP Batteries: A Synergistic Approach Using Coulomb Counting Reset, Machine Learning, and Relaxation,” *ACS Energy Letters*, vol. 10, no. 2, pp. 741–749, Feb. 2025.

[44] D. Son, Y. Song, S. Park, J. Oh, and S. W. Kim, “Online State-of-Charge and Capacity Co-Estimation for Lithium-Ion Batteries under Aging and Varying Temperatures,” *Energy*, vol. 316, p. 134434, Feb. 2025.

[45] L. Wang, J. Duan, K. Zhao, and L. Sun, “Online State of Charge Estimation of LiFePO4 Battery Based on EKF-AUKF Algorithm with Reference Compensation for Estimation Results,” *Journal of Energy Storage*, vol. 100, p. 113504, Oct. 2024.

Appendix A

Benchmark Configuration and Reproduction Details

This appendix provides the complete benchmark case definitions and common implementation settings used for the simulations presented in Chapter 5. The battery model, operating profile, pack configuration, and baseline Coulomb Counting implementation have already been introduced in Chapter 3 and are therefore not repeated here.

A.1 Complete Benchmark Case Definitions

Table A.1 lists the complete input settings for all benchmark cases evaluated in Chapter 5. The reference initial SOC denotes the initial SOC of the battery plant, whereas the estimator initial SOC is the value supplied to the Coulomb Counting estimators.

Current measurement bias was introduced only into the estimator current path and did not modify the physical current applied to the battery plant. The estimator current was defined as

$$I_{\mathrm{est}}(k) = I_{\mathrm{plant}}(k) + b_I \tag{A.1}$$

where b_I is the injected constant current bias.

Capacity mismatch was introduced by scaling the usable capacity of the battery plant:

$$Q_{\mathrm{plant}} = \gamma_Q Q_{\mathrm{nom}} \tag{A.2}$$

where γ_Q is the capacity factor listed in Table A.1.

Table A.1: Complete definitions of the benchmark cases evaluated in Chapter 5

Error group	Case	Reference initial SOC	Estimator initial SOC	Current bias (A)	Capacity factor
Baseline	A0	0.98	0.98	0.0	1.00
Initial SOC	B1	0.98	0.90	0.0	1.00
	B2	0.98	0.85	0.0	1.00
	B3	0.80	0.90	0.0	1.00
Current bias	C1	0.98	0.98	+1.0	1.00
	C2	0.98	0.98	+0.5	1.00
	C3	0.98	0.98	−0.5	1.00
Capacity mismatch	D1	0.98	0.98	0.0	0.75
	D2	0.98	0.98	0.0	0.85
Mixed errors	E1	0.98	0.98	+1.0	0.85
	E2	0.98	0.90	0.0	0.85
	E3	0.98	0.90	+0.5	1.00

Appendix B

Detailed Implementation of the SOC Correction Methods

Appendix B documents the numerical settings and implementation details of the SOC correction methods in Chapter 4.

B.1 DS-Inspired OCV Initialization

The implemented DS-inspired method uses a first-order RC approximation rather than the final second-order RC estimator of the original study. Therefore, the method is treated as an adapted benchmark implementation.

For each local current window, the terminal voltage is estimated by the first-order discrete structure

$$U_k = \theta_1 + a_1 U_{k-1} + a_2 I_k + a_3 I_{k-1}, \tag{B.1}$$

where U_k is the selected cell voltage, I_k is the estimator current, and θ_1, a_1, a_2, and a_3 are local regression coefficients. Listing B.1 shows the core implementation of this local least-squares step. The full script also contains signal loading, plotting, and diagnostic calculations, which are omitted here for clarity.

```
% Build least-squares system from local voltage-current window
Y   = Uk(2:end);
Phi = [ones(numel(Y),1), Uk(1:end-1), Ik(2:end), Ik(1:end-1)];

% Reject weakly informative or ill-conditioned windows
if range(Ik) < min_excitation_A
    continue;
end

G = Phi' * Phi;
if rcond(G) < 1/max_cond
    continue;
end

theta = G \ (Phi' * Y);

theta1 = theta(1);
a1     = theta(2);
```

```

if abs(1 - a1) < 1e-6
    continue;
end

% OCV-related estimate from the local RC approximation
Uoc_k = theta1 / (1 - a1);
```

Listing B.1: Core local LSE step used in the DS-inspired implementation.

The valid local OCV estimates are then used to fit a benchmark-specific OCV relation based on the measured voltage and current. Next, the fitted initial OCV is converted to an initial SOC using the benchmark OCV–SOC lookup table. Since the OCV–SOC relation of LFP cells contains a large plateau, the inversion is limited to a local SOC window around the SOC estimation.

After the corrected initial SOC is obtained, the method does not apply any further online corrections. The remaining SOC calculation is propagated using standard Coulomb Counting, as mentioned in (2.11).

B.2 LW Cycle-Based Correction

Listing B.2 shows the capacity-update logic used in the reproduced LW method. A capacity candidate is formed only when the cycle throughput and the anchor-implied SOC change are both sufficiently large. The candidate will be rejected if the direction is inconsistent with the SOC change or if it differs too much from the previous capacity. A separate consistency check is applied before the filtered capacity is updated.

```
Q_net_cycle_Ah = sign_dis * sum(Ik_pack .* dt) / 3600;
dSOC_cycle     = SOC0k - SOC0_next;

if abs(dSOC_cycle) >= dSOC_min && ...
        abs(Q_net_cycle_Ah) >= Ah_min

    if sign(Q_net_cycle_Ah) == sign(dSOC_cycle)
        C_tmp = abs(Q_net_cycle_Ah) / abs(dSOC_cycle);

        if isfinite(C_tmp) && C_tmp > 0 && ...
                abs(C_tmp - Cb_prev)/Cb_prev <= Cb_jump_max

            Ctmp_hist(k) = min(Cb_max, max(Cb_min, C_tmp));
        end
    end
end

[use_Cb_update, C_target] = capacity_candidate_is_stable( ...
    Ctmp_hist, k, Cb_prev, ...
    Cb_consistency_n, Cb_consistency_tol);

if use_Cb_update
    Cb_k = (1 - Cb_alpha) * Cb_prev ...
           + Cb_alpha * C_target;
    Cb_k = min(Cb_max, max(Cb_min, Cb_k));
end
```

Listing B.2: Core guarded capacity-update step in the reproduced LW method.

In the final implementation, the update requires a minimum cycle throughput of 0.2 Ah and a minimum anchor-implied SOC change of 0.01. The maximum accepted cycle-to-cycle capacity jump is 30%, and two consecutive consistent capacity candidates are required before the update is accepted. This guarded update is the reason why the LW method is most effective in the capacity-mismatch cases, and it also explains why its performance depends on reliable cycle anchors and current-based throughput.

B.3 Improved LW Bias Compensation

The improved LW strategy keeps the cycle-based structure described in Chapter 4 and adds a guarded current-bias compensation step. Listing B.3 shows the core bias-update logic. A raw bias estimate is first formed from the difference between the measured current-integrated charge and the anchor-implied charge. The estimate is accepted only when it is finite, sufficiently large, within the allowed bias range, and consistent with the previous cycle.

```
b_raw = (Q_meas_Ah - Q_anchor_Ah) * 3600 / T_cycle;
use_bias_update = false;

if isfinite(b_raw) && ...
        abs(b_raw) >= bias_braw_min && ...
        abs(b_raw) <= bhat_max

    if k >= 2
        b_raw_prev = braw_hist(k-1);

        if isfinite(b_raw_prev)
            same_sign = sign(b_raw) == sign(b_raw_prev);
            similar_mag = ...
                abs(b_raw - b_raw_prev) <= bias_braw_jump;

            use_bias_update = same_sign && similar_mag;
        end
    elseif bias_use_cycle1
        use_bias_update = true;
    end
end

if use_bias_update
    b_hat_k = (1 - bhat_alpha) * bhat_prev ...
              + bhat_alpha * b_raw;
    b_hat_k = min(bhat_max, max(bhat_min, b_hat_k));
else
    b_hat_k = bhat_prev;
end
```

Listing B.3: Core gated current-bias update in the improved LW strategy.

In the final implementation, the update is conservative. It is only allowed to update the current bias estimation when the raw bias magnitude exceeds 0.5 A, the maximum allowed cycle-to-cycle raw bias change is 0.8 A, and the filtered estimate is limited to ±5 A. These conservative guards reduce the risk of unreliable current correction based on a single cycle.

B.4 Region-Aware BCA Implementation

Listing B.4 shows the core implementation of the region-aware voltage anchor in BCA method. The local mean OCV–SOC slope is first converted into a confidence factor, and when the slope is below the plateau threshold, the confidence becomes zero and no voltage-derived SOC anchoring is applied. On the contrary, when the slope is sufficiently high, the voltage-derived SOC residual is accepted with a bounded gain.

```
slope_conf = clamp( ...
    (dVdSOC_abs_mean_cell - dvdsoc_plateau_cell) / ...
    max(dvdsoc_strong_cell - dvdsoc_plateau_cell, 1e-6), ...
    0, 1);

if slope_conf <= 0
    cyc_region_mode = "plateau_BCA_only";
else
    SOC_ocv_mean = mean(SOC_ocv_cap, 'omitnan');
    SOC_est_mean = mean(SOC_cap_anchor, 'omitnan');
    soc_residual = SOC_ocv_mean - SOC_est_mean;

    if isfinite(soc_residual) && ...
            abs(soc_residual) > soc_anchor_deadband

        alpha_V = soc_anchor_alpha_max * slope_conf;

        delta_SOC = clamp(alpha_V * soc_residual, ...
            -soc_anchor_jump_max, soc_anchor_jump_max);

        SOC_BCA(anchor_global:idx_global(end)) = clamp( ...
            SOC_BCA(anchor_global:idx_global(end)) ...
            + delta_SOC, 0, 1);
    end
end
```

Listing B.4: Core slope-gated voltage-anchor logic in the BCA-CC implementation.

Apart from the mentioned parameters, the plateau threshold is set to 0.050 V/SOC and the strong-observability threshold is set to 0.120 V/SOC. Also, the maximum voltage-anchor gain is 0.55, the SOC-anchor deadband is 0.004, and the maximum SOC correction applied at one cycle boundary is limited to 0.080. These settings are used to prevent the estimator from applying a large SOC correction in the plateau region.

The listings in this appendix show only the core fragments of each method for reproduction, and therefore the full codes are not introduced here.

Appendix C

Supplementary Simulation Results

This appendix presents one supplementary simulation case that is not analyzed in the main text. It provides additional evidence to support the conclusions drawn in Chapter 5.

C.1 Mixed Error Case with Partial Error Cancellation

Figure C.1 shows the mixed case where the plant capacity is decreased to 0.85 and the estimator initial SOC is set to 0.90. This case corresponds to the second mixed-error case in Table 5.6.

The two injected errors influence the SOC estimate in opposite directions. The capacity mismatch causes the estimator to underestimate the SOC variation for a given current interval because it assumes a larger capacity than the plant actually has. This effect tends to make the estimated SOC higher than the reference SOC during repeated cycling. In contrast, the underestimated initial SOC introduces a negative offset at the beginning of the simulation. As a result, the two errors partially compensate for each other during parts of the operating profile.

This supplementary case therefore supports the interpretation in Section 5.6: under mixed-error conditions, a low RMSE does not necessarily mean that the estimator is generally reliable. The sign and interaction of the error sources must also be considered.

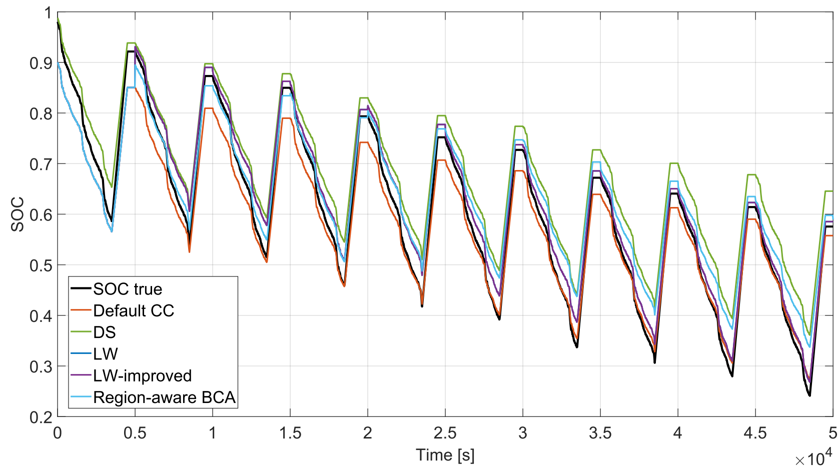

(a) SOC trajectory comparison

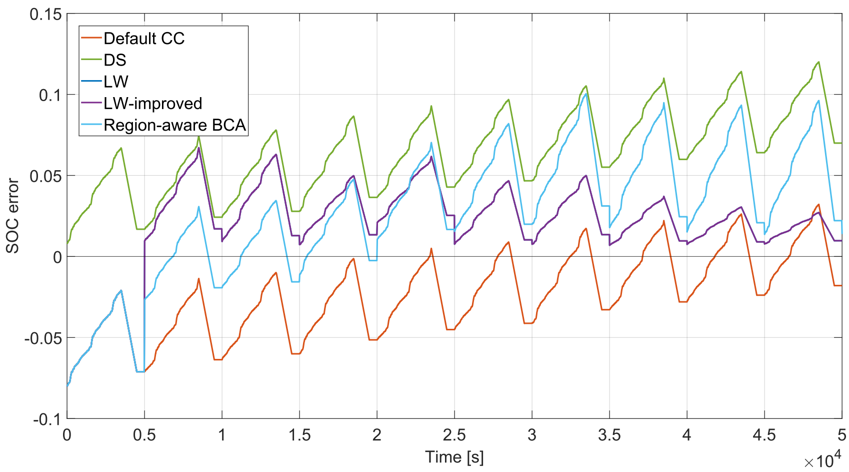

(b) SOC error comparison

Figure C.1: Supplementary SOC trajectory and error comparison for the mixed-error case with capacity factor 0.85 and estimator initial SOC 0.90.